NEUROPHYSIOLOGY

The contribution of low contrast–preferring neurons to information representation in the primary visual cortex after learning

Rie Kimura[1,2]*† and Yumiko Yoshimura[1,2]

Animals exhibit improved perception of lower-contrast visual objects after training. We explored this neuronal mechanism using multiple single-unit recordings from deep layers of the primary visual cortex (V1) of trained rats during orientation discrimination. We found that the firing rates of a subset of neurons increased by reducing luminance contrast, being at least above basal activities at low contrast. These low contrast–preferring neurons were rare during passive viewing without training or anesthesia after training. They fired more frequently in correct-choice than incorrect-choice trials. At single-neuron and population levels, they efficiently represented low-contrast orientations. Following training, in addition to generally enhanced excitation, the phase synchronization of spikes to beta oscillations at high contrast was stronger in putative inhibitory than excitatory neurons. The change in excitation-inhibition balance might contribute to low-contrast preference. Thus, low-contrast preference in V1 activity is strengthened in an experience-dependent manner, which may contribute to low-contrast visual discrimination.

INTRODUCTION

Animals can easily perceive visual objects that are repeatedly encountered (*1*–*3*). Perceptual learning improves the behavioral contrast sensitivity, leading to a high ability to detect the experienced stimulus, even if it becomes vague (*4*). Human functional magnetic resonance imaging studies have demonstrated that activities in the primary visual cortex (V1) are strengthened by learning (*5*, *6*). The perceptional improvements are thought to be based on changes in the visual response properties of cortical neurons depending on the experience (*2*, *7*–*11*). A previous study showed that contrast sensitivity of individual neurons in cat V1 is improved after perceptual learning (*12*).

In general, the response strength of V1 neurons monotonically increases by increasing the stimulus contrasts and reaches a saturation level, while the preferred orientation of these neurons is constant irrespective of the stimulus contrasts (*13*–*16*). However, previous reports have found that some neurons in monkey V1/V2 and V4 (*17*, *18*) and mouse V1 (*19*–*22*) show preference to a certain luminance contrast. In mouse V1, neuronal population activities representing visual information are different between high- and low-contrast stimuli (*21*). These contrast preferences may contribute to the perception of various contrast stimuli, including low contrast, but this remains poorly understood.

Orientation representations in single neurons and neuronal populations in mouse V1 are improved by learning to perform a visual discrimination task (*10*). Top-down inputs from higher cortical areas (*9*, *23*) and modulatory inputs (*24*) are responsible for the improvement of orientation representations. In addition, inhibitory interneurons contribute to the improvement of neuronal orientation representations in V1 after learning (*8*). Previous studies have demonstrated that the improved neuronal representations of visual information are the basis of good performance of visual discrimination (*8*, *9*, *23*–*25*). Therefore, to understand the learning-dependent neuronal mechanisms underlying the perception of low-contrast visual stimulation, it is important to clarify the changes in visual information representations depending on luminance contrasts after learning. However, it remains unknown whether contrast preferences in V1 neurons are modified by learning and, if so, whether the modified neuronal activities represent visual information and relate to visual behavioral performance improved by training.

In this study, we performed multiple single-unit recordings from rat V1 during an orientation discrimination task at different contrasts. We demonstrated that the low-contrast preference of visually evoked enhanced (above basal activities)–type responses is strengthened after learning. These low contrast–preferring neurons represented separately two different orientations at low contrast. Thus, low contrast–preferring neurons could have an important role in perception of familiar visual objects even if the objects become obscured.

RESULTS

Multiple single-unit recordings during an orientation discrimination task

To explore the neuronal mechanisms enabling the discrimination of vague stimuli after training, we analyzed spiking activities in V1 of adult rats during an orientation discrimination task (Fig. 1A). Head-restrained rats were trained to push or pull a lever with their forelimb depending on whether the presented high-contrast (contrast, 100%) sinusoidal grating stimuli were vertical or horizontal, respectively. This two-alternative forced-choice task allowed us to measure the visual acuity without omission trials (*14*). The percentages of correct answers were significantly above the chance level (50%) in the seventh to ninth training sessions and increased further with additional training (Fig. 1B and fig. S1A). After achievement of high

[1]Division of Visual Information Processing, National Institute for Physiological Sciences, National Institutes of Natural Sciences, Okazaki, Japan. [2]Department of Physiological Sciences, SOKENDAI (The Graduate University for Advanced Studies), Okazaki, Japan.
*Corresponding author. Email: kimurar@m.u-tokyo.ac.jp
†Present address: Department of Physiology, Graduate School of Medicine, The University of Tokyo, Tokyo, Japan.

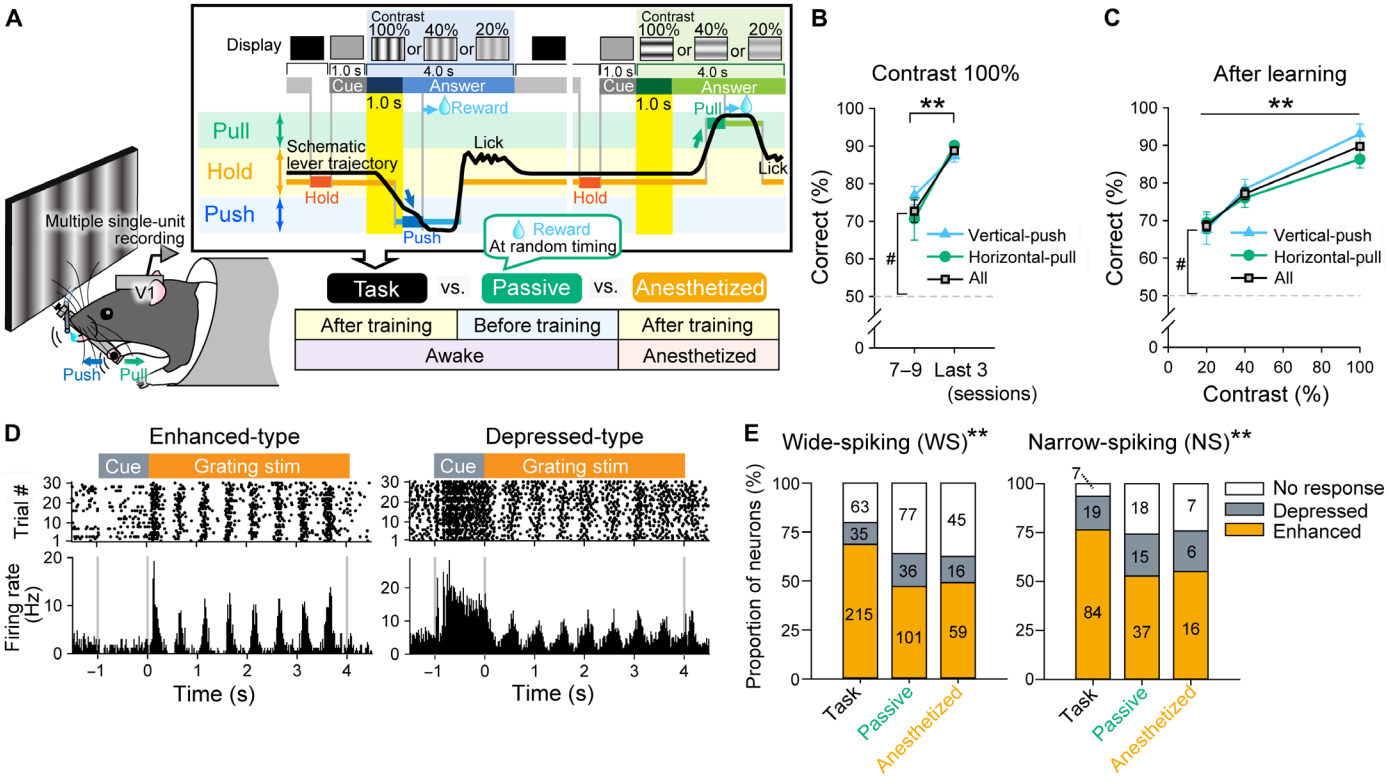

Fig. 1. Visual responses during the orientation discrimination task. (**A**) Behavioral task. Head-restrained rats were rewarded for performing the correct movement (push or pull) depending on the orientation (vertical or horizontal) of drifting sinusoidal gratings with three contrasts (20, 40, and 100%) after training. Neuronal activities were analyzed for the first 1 s during the grating presentation in the task, passive, and anesthetized groups (yellow box). (**B**) Performance improvements with training using the 100% contrast stimuli (25 ± 4 sessions in total, $N = 7$ rats). The percentages of correct responses were significantly above the 50% chance level during the seventh to ninth sessions (after 1-week discrimination training; Holm-corrected #$P < 0.05$, one-sample signed-rank test). The percentages of correct responses were further improved with training sessions (during the last three sessions; vertical, 87.4 ± 1.7%; horizontal, 90.2 ± 0.7%; all, 88.8 ± 1.0%; **$P < 0.001$, Friedman's test). (**C**) Population average percentages of correct responses versus stimulus contrasts after sufficient training. The correct ratios decreased with the decreasing contrast (**$P < 0.001$, Friedman's test; $N = 7$ rats). The correct ratios at the 20% contrast stimuli were above the chance level (Holm-corrected #$P < 0.05$, one-sample signed-rank test). (**D**) Two types of firing patterns during task performance. Visual stimuli increased the firing rates (enhanced-type, left) or decreased them (depressed-type, right). Raster plots (extracted 30 trials; top) and peristimulus time histograms (PSTHs; bottom) were aligned to grating stimulus (stim) onset. (**E**) Proportions of neurons showing enhanced-type and depressed-type firings, and no visual responses, in the task, passive, and anesthetized groups. The number of neurons is shown in the bar. The proportion was significantly different among the three groups in WS neurons (left; **$P < 0.001$, chi-square test) and NS neurons (right; **$P = 0.002$).

correct percentages, stimulus contrast was reduced (20 and 40%) in half of the trials to make visual discrimination more difficult. The correct percentages became lower by reducing the contrast, although the percentages at 20% contrast were still significantly higher than chance (Fig. 1C). On the basis of the proportion of correct answers in an orientation discrimination behavioral task (Fig. 1C) (*24*), the 20% contrast stimuli should be regarded as the low-contrast stimuli, although 20% contrast is not low for a contrast detection task (*26*). During recording in a session, rats performed the task at a steady pace (fig. S1B).

We performed multiple single-unit recordings from deep layers in V1 (fig. S1C) during task performance after sufficient training (task group; Fig. 1A). Neuronal activities were also recorded from untrained rats during passive viewing (passive group) or trained rats under anesthesia (anesthetized group). We classified recorded units into wide-spiking (WS; putative excitatory) and narrow-spiking (NS; putative inhibitory) neuron-derived ones on the basis of the spike width (fig. S1, D, F, and H). Figure 1D shows representative firing patterns in two WS neurons during task performance with the 100% contrast sinusoidal gratings of the preferred orientation at a temporal frequency of 2 Hz. Visually responsive neurons were determined according to the differences in firing rates between the period of cue presentation and that of grating stimulation. Most of the visually responsive neurons in the task group showed increased firing rates during grating stimulation with at least one combination of stimulus parameters (orientation and contrast), compared with cue presentation (enhanced type, 68.7% among WS neurons, 76.4% among NS neurons). The other neurons showed only decreased firing rates during grating stimulation with any combination of parameters (depressed type; Fig. 1D) (*8*, *27*–*30*). Information representation must be quite different between them. For example, a previous paper revealed that depressed-type neurons in V1 have less task-relevant selectivity than enhanced-type neurons, suggesting that the depressed-type activities might reduce any ongoing task-irrelevant activity and improve the readout of task-relevant population activity by higher-order neurons (*27*). Therefore, we classified enhanced-type and depressed-type neurons. The proportion of enhanced-type neurons among both WS and NS neurons was higher in rats of the task group than in those of the passive or anesthetized

group (Fig. 1E). The result was consistent across animals and recording sessions (fig. S1, E, G, and I). On the other hand, the proportion of depressed-type neurons was low and not considerably different among these three groups of rats. Therefore, in this study, we hereafter focused on the enhanced-type neurons, unless otherwise specifically noted.

Low-contrast preference in V1 activity during task performance

To examine contrast-dependent changes in spiking activities during visual discrimination, we analyzed the enhanced-type responses to visual stimuli with preferred orientation (vertical or horizontal) at three different contrasts (100, 40, and 20%) in the correct trials during the task. We observed that firing rates became higher in some WS neurons by increasing the stimulus contrast (high-contrast preference; Fig. 2A). Notably, other WS neurons showed higher firing rates when the stimulus contrasts were decreased (low-contrast preference; Fig. 2B). Figure 2C shows the time courses of firing rates [peristimulus time histograms (PSTHs)] at each stimulus contrast in individual enhanced-type WS neurons. The PSTHs were normalized by the maximum firing rates at the preferred contrast after subtraction of the activity during cue presentation. To quantify the contrast preference, we calculated the contrast selectivity index (CI[$R_{con100\%}$, $R_{con20\%}$]) on the basis of responses to the preferred orientation at 100 and 20% contrast in individual neurons. When the PSTHs were sorted by the CIs, we noticed that a subset of WS neurons showed low-contrast preference (39.1%, 84 of 215 neurons; CI < 0). Similar to enhanced-type WS neurons, 46.4% of enhanced-type NS neurons showed low-contrast preference (39 of 84 neurons; Fig. 2D). For high or low contrast–preferring neurons showing statistical significance ($P < 0.05$, Wilcoxon rank sum test), the peak time-aligned averages of normalized PSTHs at 100 and 20% contrast were constructed (for WS neurons, Fig. 2E; NS neurons, Fig. 2F). The separation of high- and low-contrast preference did not depend on the strength of visual responses (fig. S2A). In both significantly high and low contrast–preferring neurons, the firing rates at 40% contrast showed intermediate values between those at 100 and 20% contrast on average, although there were some exceptions showing high activities at 40% contrast (fig. S2B).

The CIs were distributed in a wide range, including positive and negative values, in both enhanced-type WS and NS neurons during the task (Fig. 3A). As stated above, while the CI value was positive when the firing rate at 100% contrast was higher than that at 20%, it was negative when the firing rate at 20% contrast was higher than that at 100%. The distribution was significantly different from the hypothesized chance-level distribution bootstrapped with replacements in the 100 and 20% contrast stimulus trials (WS and NS; $P < 0.001$, one-sample Kolmogorov-Smirnov test; Fig. 3B). In 16.7% of WS neurons and 20.2% of NS neurons, the firing rate at 20% contrast was significantly higher than that at 100% contrast (Fig. 3, A and G). These proportions were also significantly above the chance level (WS and NS; $P < 0.0001$, bootstrap test). The results were consistent across animals and recording sessions (fig. S2C). Low and high contrast–preferring neurons were simultaneously recorded using multichannel electrodes in each session (fig. S2C). Thus, it is unlikely that low-contrast preference is directly related to peripheral effects such as pupil size (*31*) and contrast gain control in retinal cells (*32*, *33*).

In WS and NS neurons, the spike widths did not statistically differ between significantly low and high contrast–preferring neurons

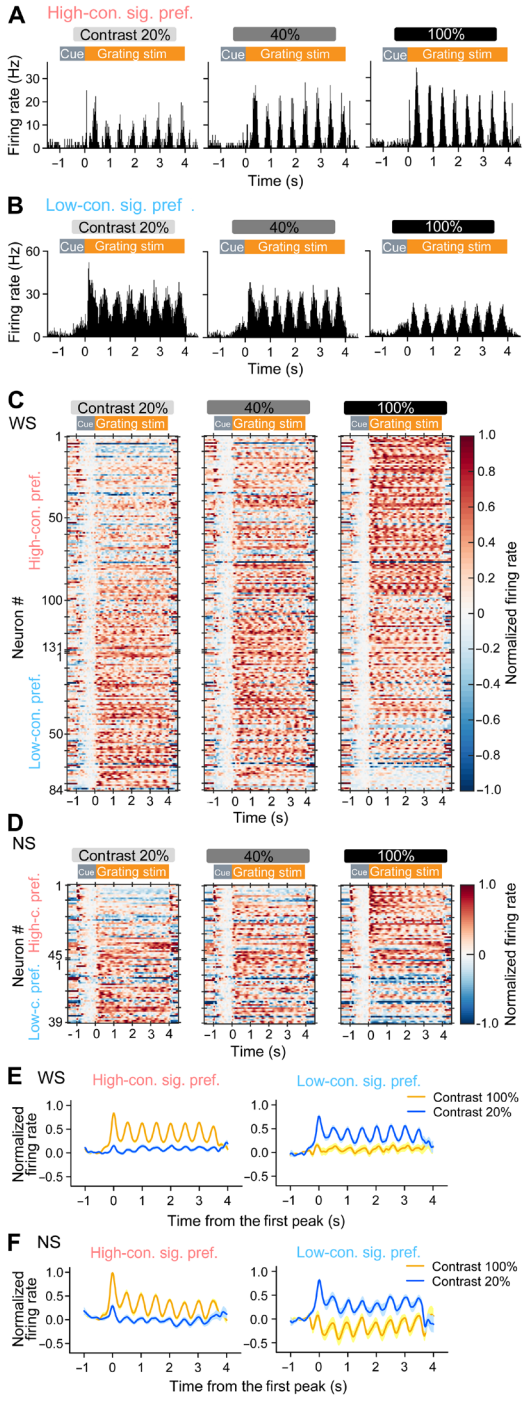

Fig. 2. Contrast preference of neurons with enhanced-type spiking activities during the orientation discrimination task. (**A** and **B**) Representative PSTHs of WS neurons exhibiting high-contrast (A) ($P < 0.001$ for contrast 20% versus 100%, Wilcoxon rank sum test) or low-contrast significant preference (B) ($P < 0.001$). (**C** and **D**) Individual pseudo-colored PSTHs normalized by peak responses after subtracting cue responses in WS (C) ($n = 215$) and NS neurons (D) ($n = 84$). Responses to the preferred orientation were shown. The PSTHs were sorted in descending order according to the CI. (**E**) The peak time–aligned population averages of normalized PSTHs of significantly high ($n = 84$) and low ($n = 36$) contrast–preferring WS neurons ($P < 0.05$, Wilcoxon rank sum test). (**F**) Similar to (E), but NS neurons (high-con. sig. pref., $n = 26$; low-con. sig. pref., $n = 17$). High-con. sig. pref., high-contrast significant preference; Low-con. sig. pref., low-contrast significant preference.

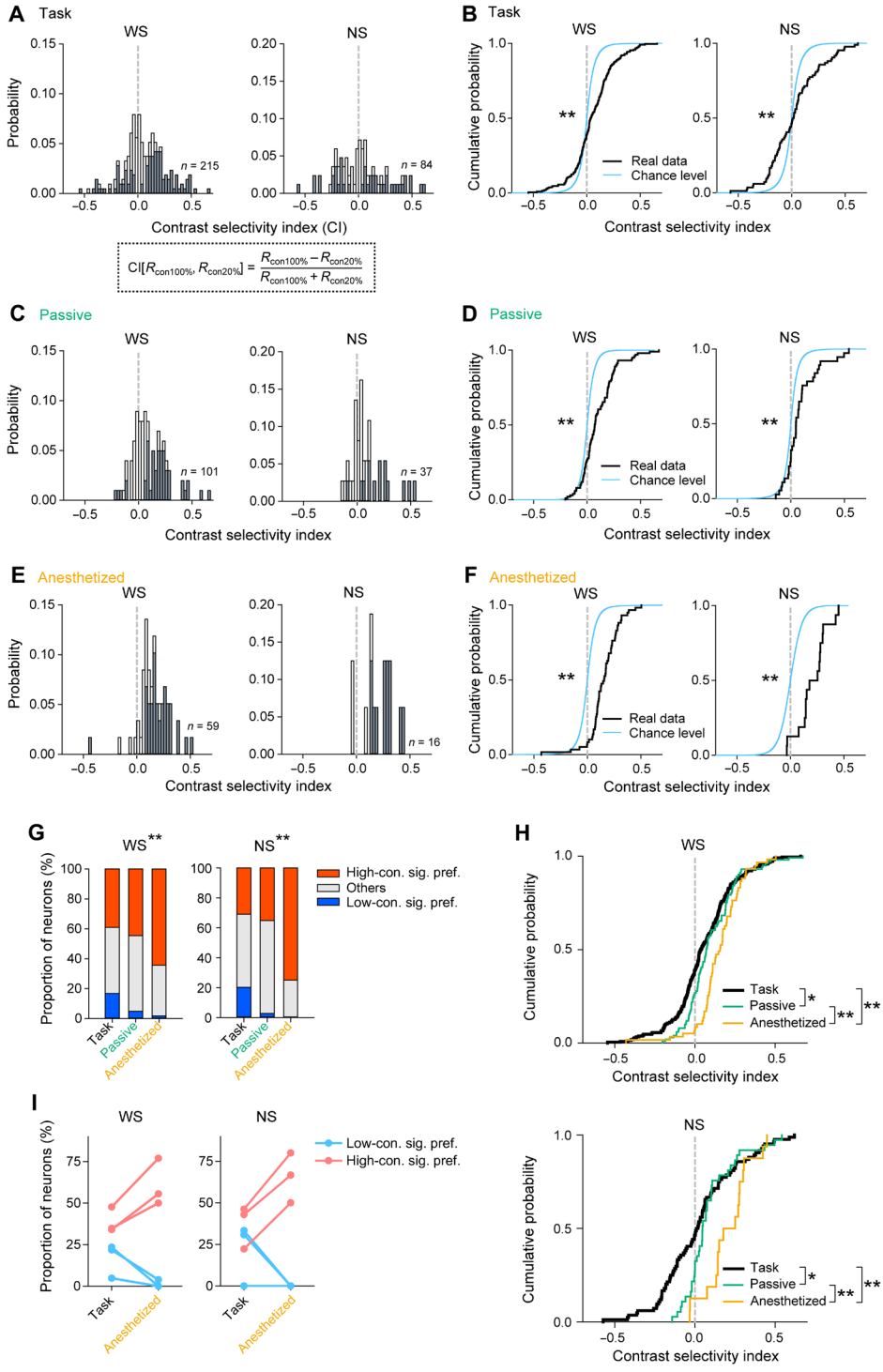

Fig. 3. Contrast dependence of visual responses in the task, passive, and anesthetized groups. (**A**) Histograms of the CIs of WS (left) and NS (right) neurons with enhanced-type spiking activities in the task group. The CI was calculated on the basis of responses to the preferred orientation at 100 and 20% contrast. Gray bars represent the probability of neurons with significant differences in responses between the 100 and 20% contrast stimuli ($P < 0.05$, Wilcoxon rank sum test). The number of analyzed neurons is shown in the histogram. (**B**) Cumulative CI distributions of real data and hypothesized trial-shuffled chance-level bootstrap data in WS (left) and NS neurons (right). $^{**}P < 0.001$, one-sample Kolmogorov-Smirnov test. (**C** and **D**) Similar to (A) and (B), but in the passive group without training. (**E** and **F**) Similar to (A) and (B), but under anesthesia in trained rats. (**G**) Comparisons of proportions of neurons with significant ($P < 0.05$) contrast preference to either contrast among the task, passive, and anesthetized groups. WS: $^{**}P < 0.001$, chi-square test; NS: $^{**}P < 0.001$. (**H**) Comparisons of CIs among the task, passive, and anesthetized groups. The data were the same as real data in (B), (D), and (F). Holm-corrected $^{**}P < 0.01$ and Holm $^{*}P < 0.05$, Kolmogorov-Smirnov test. (**I**) Changes in the proportions of neurons with significant contrast preference ($P < 0.05$) between the period of task performance and anesthesia in the same rats ($N = 3$ rats). Note that significantly low contrast–preferring neurons disappeared after applying anesthesia.

in the task group (fig. S3A). In addition, the linearity of response to drifting sinusoidal stimuli was calculated as the periodic modulation of the firing relative to the average firing rate, i.e., the $F1/F0$ ratio. This ratio did not differ between low and high contrast–preferring neurons, suggesting that low-contrast preference was independent of whether the neuron was a simple or complex cell (fig. S3B) (*15*, *20*). Excitatory neurons in deep layers comprise both regular-spiking and burst-spiking types (*34*, *35*). Both types were observed in low and high contrast–preferring WS neurons (fig. S3C). These results suggest that low-contrast preference is independent of neuron subtypes classified in this study.

To examine whether training and brain state affect the emergence of low-contrast preference of enhanced-type activities, we also analyzed contrast preference in the passive and anesthetized groups (Fig. 1A). In these two groups, most of WS and NS neurons showed high-contrast preference (Fig. 3, C and E, and fig. S2, D to I). The distribution of the CIs was different from the chance-level distribution because of the shift only toward positive values (Fig. 3, D and F). The proportion of neurons showing low-contrast significant preference was less than 5% (Fig. 3G) and was not significantly above the chance level in the passive (WS, 4.95%, $P = 0.1085$; NS, 2.70%, $P = 0.6104$, bootstrap test) and anesthetized groups (WS, 1.69%, $P = 0.7707$; NS, 0.00%, $P = 1.0000$). The distribution of CIs in the task group was significantly shifted to negative values compared to that in the passive and anesthetized groups, demonstrating that low-contrast preference was observed preferentially in the task group (Fig. 3H). The proportion of low contrast–preferring neurons in trained rats remarkably decreased after administrating an anesthetic to the same animals (Fig. 3I). These results demonstrated that low-contrast preference emerged specifically in the awake state after training, commonly in WS and NS neurons.

We examined how much the CIs were affected by many kinds of factors using multiple linear regression analysis (fig. S4, A and B). The visual responses were strongly affected by the presented contrast in the trial and were not so affected in a certain direction by the other factors. Furthermore to confirm the result, that we examined the correlation of the CIs for subpopulations with and without a factor (fig. S4, C to F). The CIs in the first half of the trials within a recorded session were strongly correlated to those in the second half in WS and NS neurons of rats in the task group (fig. S4C). The CIs were not affected by the presence or absence of lever movements within the visual response analysis window (fig. S4D) or reward consumption immediately before the visual stimulus presentation (fig. S4E). In addition, the CIs were not affected by the visual contrast presented in the previous trial (fig. S4F). This evidence suggests that contrast preference was not mostly determined by the contrast aftereffects or adaptation (*28*). So far, we had used visual responses during the first 1-s stimulation for calculating the CIs. However, as expected from the robustness, the CIs for the first 1-s and whole 4-s responses were strongly similar (fig. S4G). Furthermore, when the responses were selected to make the variability uniform in the task and passive groups, low-contrast preference in the task group was maintained (fig. S4, H to J). These results indicate the robustness of contrast preference.

Relationship between neuronal activities and behavioral task performance

Low contrast–preferring enhanced-type activities were observed preferentially during task performance. This raises the possibility that the activities are involved in behavioral orientation discrimination, particularly at low-contrast stimuli. To test this, we compared neuronal activity during task performance with the 20% contrast stimuli between correct and incorrect trials. The performance selectivity index (PI[$R_{correct}$, R_{error}]) in individual neurons was calculated on the basis of visual responses to preferred orientation in these trials (Fig. 4). Positive and negative values in PI reflected stronger activity in correct and incorrect trials, respectively. In WS and NS neurons with low-contrast preference (CI ≤ -0.025), the distribution of PIs was significantly skewed toward positive values compared with the hypothesized chance-level distribution (Fig. 4, A and B). However, the distribution in high contrast–preferring neurons (CI ≥ 0.025) did not significantly differ from the chance-level distribution (Fig. 4C). PIs were significantly higher in low than in high contrast–preferring neurons (Fig. 4D). Thus, low contrast–preferring neurons fired more strongly in correct than incorrect trials, whereas high contrast–preferring neurons did not.

Low-contrast preference in enhanced-type activity of WS and NS neurons was also observed when nonpreferred (orthogonal) orientation stimuli were presented in the task group (fig. S5, A to E). The CIs for preferred and nonpreferred orientations were highly correlated (fig. S5, F to H). However, the distribution of PIs calculated from responses to nonpreferred orientation did not significantly differ from the chance-level distribution both in low and in high contrast–preferring neurons in the task group (fig. S6, A to C). This demonstrates that responses to the nonpreferred orientation did not correlate with the behavioral performance.

We also observed low-contrast preference in depressed-type spiking activity, which showed higher activities in response to low-contrast than high-contrast stimuli, in the task, passive, and anesthetized groups (fig. S7, A to L). However, the distribution of CIs was similar among the task, passive, and anesthetized groups (fig. S7L). The distribution of PIs did not significantly differ from the chance-level distribution (fig. S7M). Thus, only responses to the preferred orientation in the low contrast–preferring neurons with enhanced-type activities may contribute to improving orientation discrimination at low contrast.

Orientation representations at the single-neuron level

To test the ability to represent visual stimulus features at the single-neuron level, we quantified the discriminability between vertical and horizontal orientations as the *d*-prime, calculated using visual responses in correct trials during task performance in individual enhanced-type WS and NS neurons showing significant preference to either contrast (Fig. 5A). In both neuron types, the orientation discriminability at each tested contrast was above the shuffled chance level irrespective of low- or high-contrast preference (Holm-corrected $P < 0.01$, Wilcoxon rank sum test). The discriminability at 20% contrast was higher in low than in high contrast–preferring neurons, while that at 40 or 100% contrast did not differ (Fig. 5A). These results suggest that, while single low and high contrast–preferring neurons separately represent two orientations, the low contrast–preferring neurons are particularly related to the low-contrast orientation representations.

Furthermore, orientation discriminability of significantly low contrast–preferring enhanced-type neurons at 20% contrast was recalculated more rigorously by holding the parameters other than the orientations concerned (fig. S8A). The orientation discriminability was calculated in the trials of the same movements (push or

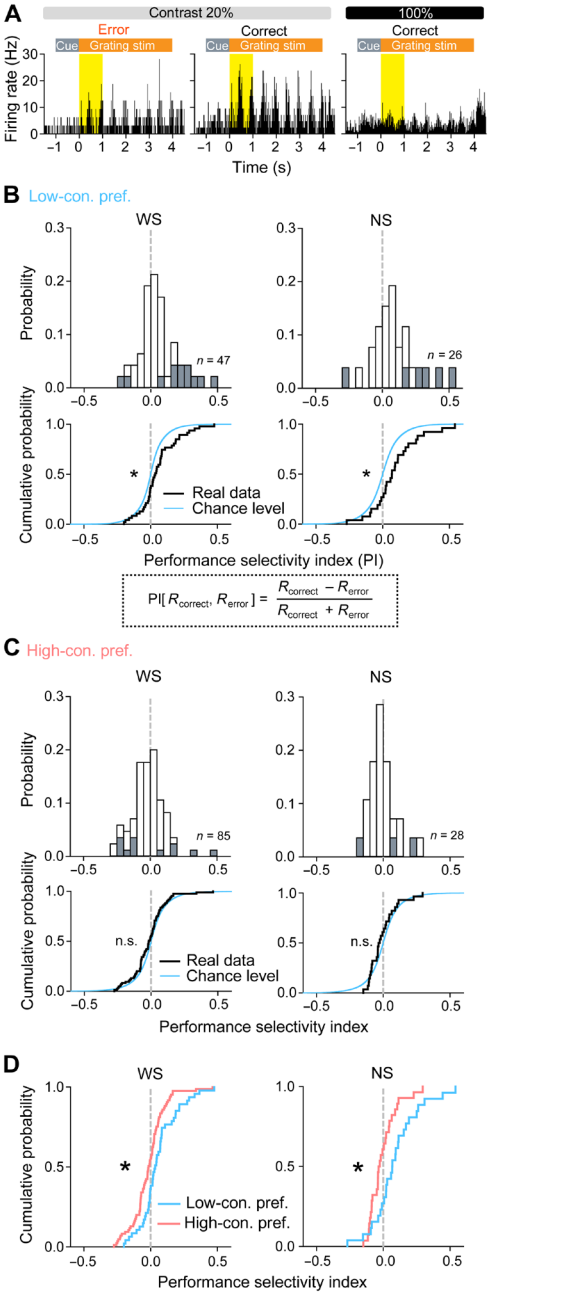

Fig. 4. Task performance–related activities of low contrast–preferring neurons. (**A**) Representative PSTHs of a low contrast–preferring enhanced-type WS neuron (CI = −0.326) exhibiting significant preference of activities for correct to incorrect trials at 20% contrast ($P = 0.022$, Wilcoxon rank sum test). The yellow box shows the time window for analysis. (**B**) Top: Histograms of PIs in enhanced-type WS (left) and NS neurons (right) with low-contrast preference (CI ≤ −0.025). The PI was calculated on the basis of responses to the preferred orientation in correct-choice and incorrect-choice trials. Gray bars represent the probability of neurons with significant differences in responses between correct and incorrect trials ($P < 0.05$, Wilcoxon rank sum test). The number of analyzed neurons is shown in the histogram. Bottom: Comparison of cumulative PI distributions between real data and hypothesized trial-shuffled chance-level bootstrap data. *$P = 0.026$ for WS neurons and *$P = 0.010$ for NS neurons, one-sample Kolmogorov-Smirnov test. (**C**) Similar to (B), but high contrast–preferring neurons (CI ≥ 0.025). n.s., $P > 0.05$. (**D**) Comparisons of PIs between low contrast (CI ≤ −0.025)– and high contrast (CI ≥ 0.025)–preferring enhanced-type neurons. The data are the same as real data in (B) and (C). *$P = 0.018$ for WS neurons and *$P = 0.034$ for NS neurons, Kolmogorov-Smirnov test.

pull) by including not only correct but also incorrect trials. As a result, this orientation discriminability (vertical versus horizontal) was large compared with the movement discriminability (push versus pull) in presenting the same orientation (fig. S8A). Thus, it was confirmed that low contrast–preferring neurons substantially represented the orientation information at low contrast. Next, the orientation discriminability had been expected to depend on task performance, on the basis of the PIs at preferred and nonpreferred orientations in low contrast–preferring neurons (Fig. 4B and fig. S6A). However, orientation discriminability in significantly low contrast–preferring enhanced-type neurons did not correlate with the behavioral performance at 20% contrast (fig. S8B). This contradiction may possibly be related to a little time instability of task performance–dependent visual responses (fig. S6, D and E; cf. fig. S4C).

We next explored whether the absolute differences in responses between vertical and horizontal stimulation (the numerator in *d*-prime calculation) and/or trial-to-trial variabilities (the pooled SDs; the denominator) are important factors for discriminating the two orientations. The differences in responses between the two orientations at 20% contrast were larger in low than in high contrast–preferring neurons, while this difference at 100% contrast was indistinguishable between them (Fig. 5B), consistent with *d*-prime results (Fig. 5A). The pooled SDs for visual responses at 20% contrast were higher in low than in high contrast–preferring neurons (Fig. 5C), which does not cause high *d*-prime values at 20% contrast in the former. Thus, differences in response magnitude to vertical and horizontal stimulation could be responsible for *d*-prime in the task group.

We showed that low-contrast orientation representation was better in low contrast–preferring enhanced-type neurons than high contrast–preferring neurons in the task group (Fig. 5A). We next asked whether orientation representation is improved in high contrast–preferring neurons during task performance after training. To this end, *d*-prime at each contrast was calculated in significantly high contrast–preferring neurons in the passive and anesthetized groups (Fig. 5D). The *d*-prime values in high contrast–preferring neurons of these two groups were significantly above the shuffled chance level at all the contrasts in both WS and NS neurons (NS, anesthetized, Holm-corrected $P < 0.05$ for 20 or 40% contrast, Wilcoxon rank sum test; the others, Holm $P < 0.01$). We compared these *d*-prime values with the values in significantly high contrast–preferring neurons of the task group. In WS neurons, *d*-prime values at the two lower contrasts (20 and 40%) were significantly higher in the task group than in the passive group, but the value at 100% contrast was not different between them (Fig. 5D, left). This result suggests that low-contrast orientation representation by high contrast–preferring neurons is also improved after training. In the case of NS neurons, high contrast–preferring neurons did not show a difference in *d*-prime values at 20% contrast between the task and passive groups, indicating that representations of low-contrast orientations were not improved after training (Fig. 5D, right). On the other hand, *d*-prime values at 100% contrast were significantly higher in the task group than in the passive group. Together, in high contrast–preferring neurons, high-contrast orientation representation was improved after training in NS neurons, while low-contrast orientation representation was improved in WS neurons. In addition, for both WS and NS neurons, the *d*-prime values at all tested contrasts were significantly lower in the anesthetized group than in the task group (Fig. 5D). These results demonstrate that orientation representation in high contrast–preferring neurons was also better during the task.

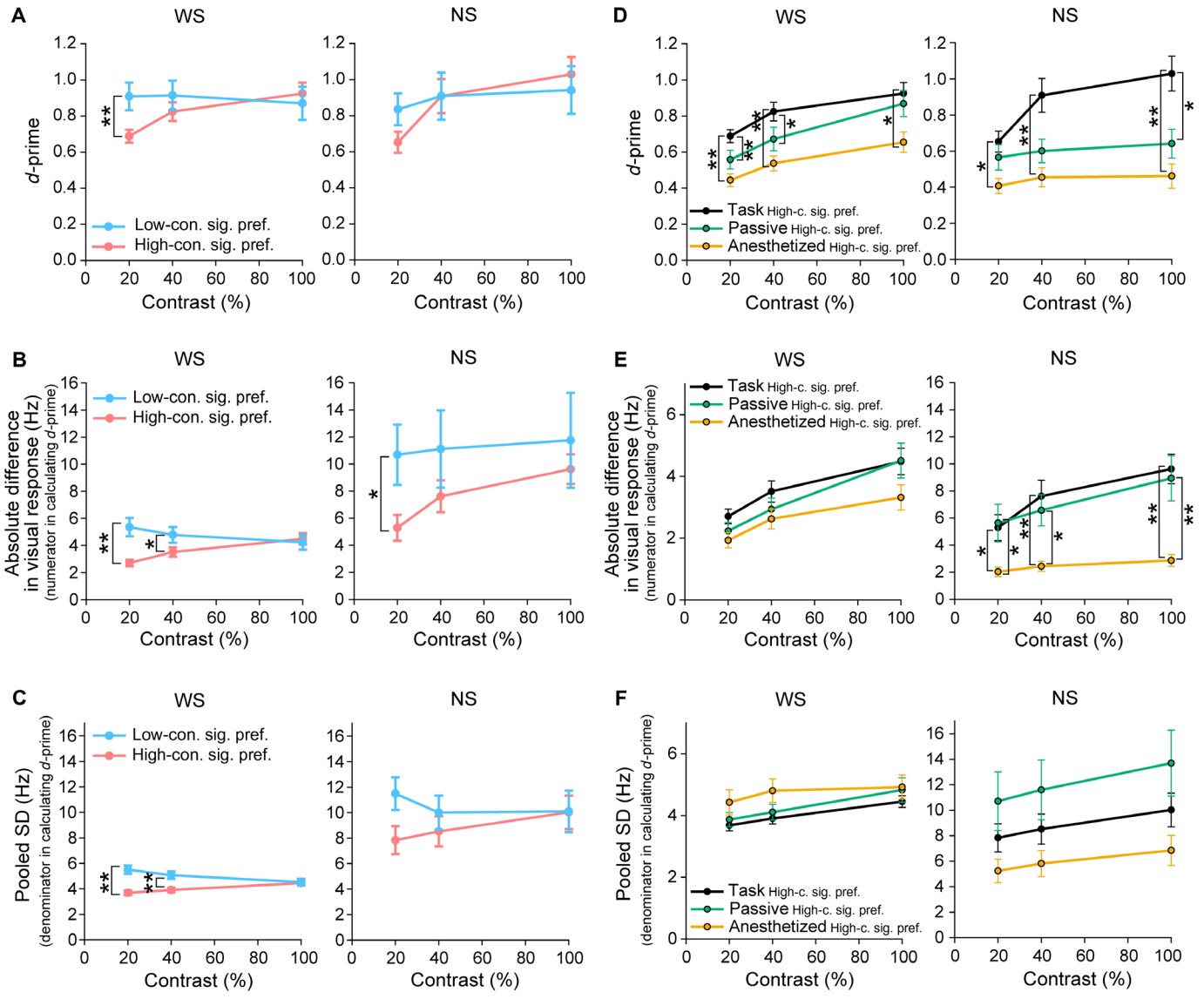

Fig. 5. Orientation discriminability at the single-neuron level. (**A**) Comparison of orientation discriminability (*d*-prime) during task performance between significantly low contrast–preferring ($P < 0.05$, Wilcoxon rank sum test; WS, $n = 36$; NS, $n = 17$) and high contrast–preferring enhanced-type neurons (WS, $n = 84$; NS, $n = 26$). Population average of *d*-prime versus stimulus contrasts. (**B**) Comparison of the absolute difference in responses to vertical and horizontal orientations (the numerator in calculating *d*-prime). (**C**) Comparison of pooled SD of orientation responses (the denominator in calculating *d*-prime). Holm-corrected $^{**}P < 0.01$ and Holm $^{*}P < 0.05$ between neuron groups showing each angle bracket in (A) to (C), Wilcoxon rank sum test. (**D**) Comparison of *d*-prime in significantly high contrast–preferring enhanced-type neurons ($P < 0.05$, Wilcoxon rank sum test) among the task (WS, $n = 84$; NS, $n = 26$), passive (WS, $n = 45$; NS, $n = 13$), and anesthetized groups (WS, $n = 38$; NS, $n = 12$). (**E**) Comparison of the numerator in *d*-prime. (**F**) Comparison of the denominator in *d*-prime. $^{**}P < 0.01$ and $^{*}P < 0.05$ between neuron groups showing each angle bracket in (D) and (E), Dunn's test after confirming the significant difference (Holm $P < 0.05$) by Kruskal-Wallis test.

The absolute differences in responses between vertical and horizontal stimulation (numerators in calculating *d*-prime) and the pooled SDs (denominators) in the passive and anesthetized groups are shown in Fig. 5 (E and F). The numerators and the denominators were slightly low or high in the passive or anesthetized group, compared with the task group. These combined differences may lead to the significantly higher *d*-primes in the task group.

Orientation representations at the population level

To examine whether the accuracy of orientation representations by the neuronal population on a trial-to-trial basis changed after training, we performed a decoder analysis using the nearest-centroid decoder (Fig. 6) (*36*, *37*). For this analysis, we pooled the population activities of WS and NS neurons that showed not only enhanced-type responses but also depressed-type responses and no considerable visual responses (see Fig. 1E), to analyze responses in an unbiased population of V1 neurons. The single-trial population activity from 12 randomly selected neurons for two periods (0 to 0.5 s and 0.5 to 1.0 s after the onset of grating stimuli) was expressed by a high-dimensional vector (24-dimensional vector; 12 neurons × 2 time points) (Fig. 6A), and this selection procedure was repeated 100 times. The centroid for each orientation was calculated for every stimulus contrast by

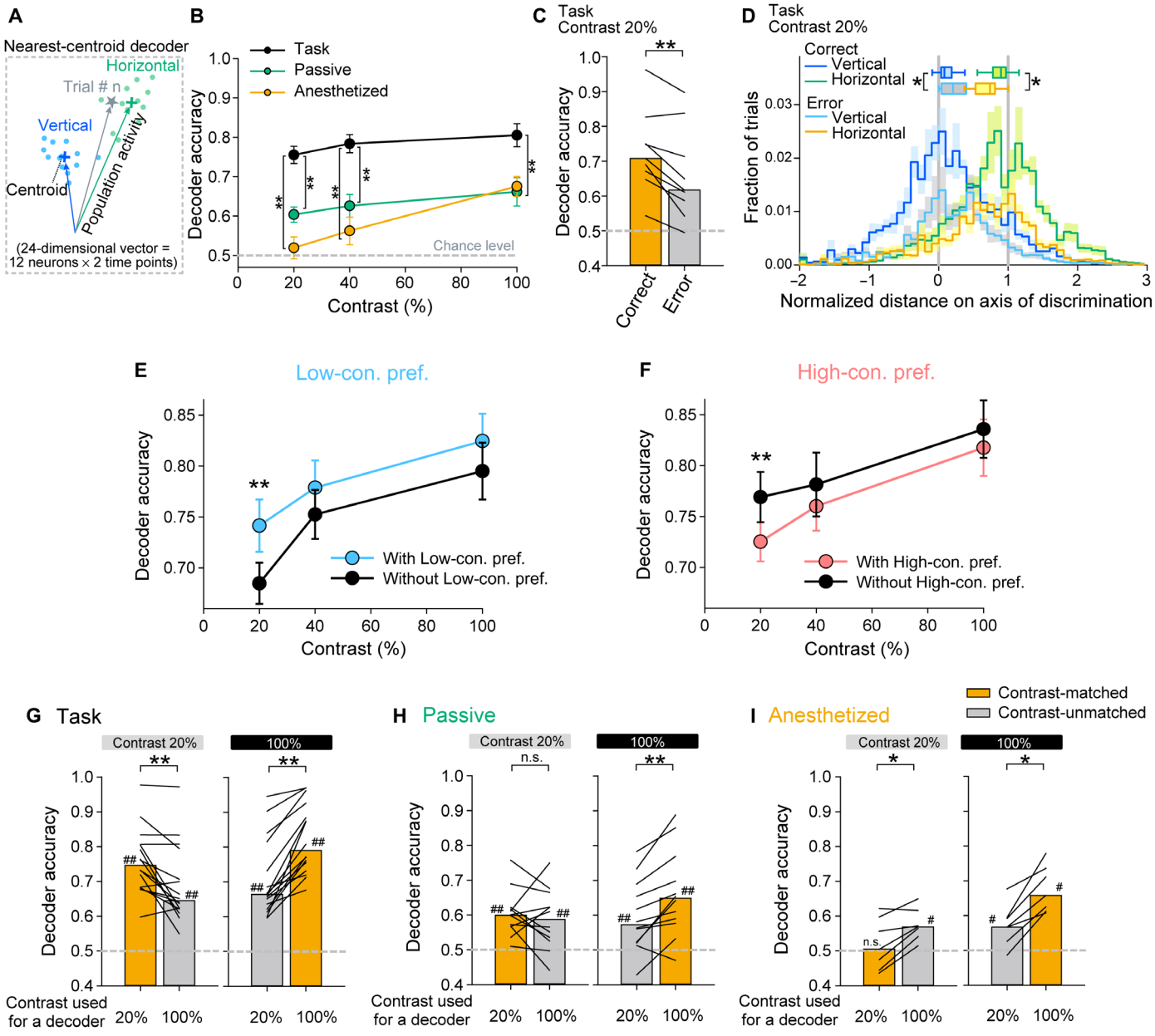

Fig. 6. Contrast-dependent orientation representation at the neuronal population level. (**A**) Schematic diagram for the nearest-centroid decoder. (**B**) Decoder accuracies versus stimulus contrasts in the task ($n = 17$ sessions), passive ($n = 12$), and anesthetized ($n = 7$) groups. $^{**}P < 0.01$, Dunn's test after Kruskal-Wallis test (Holm-corrected $P < 0.01$). (**C** and **D**) Relationship between behavioral choices and decoder accuracies during the task using the 20% contrast stimuli ($n = 9$ sessions). (C) Decoder accuracies for each session and their median value. The decoder was generated using spikes in the correct trials. $^{**}P = 0.008$, Wilcoxon signed-rank test. (D) Session-averaged histograms of the normalized distances from the vertical centroid to the test trial vector projected onto the axis connecting the vertical and horizontal centroids (shaded area, SEM). Box plot summary of the median values of the distance. Holm $^{*}P < 0.05$, Wilcoxon signed-rank test. (**E**) Comparison of accuracies for decoders with and without low contrast–preferring enhanced-type neurons (CI ≤ −0.025) during the task ($n = 13$ sessions). Holm $^{**}P < 0.01$, Wilcoxon signed-rank test. (**F**) Similar to (E), but for decoders with and without high contrast–preferring enhanced-type neurons (CI ≥ 0.025; $n = 11$). Holm $^{**}P < 0.01$. (**G**) The effect of mismatch of the stimulus contrast between decoder calculations and test trials in the task group. Left: Decoder accuracies for the 20% contrast test trials using the decoder based on responses to 20% (matched condition) or 100% contrast (unmatched condition) ($n = 16$ sessions; $^{**}P = 0.001$, Wilcoxon signed-rank test) and their median value. Right: Decoder accuracies for the 100% contrast test trials ($^{**}P < 0.001$). Holm $\#\#P < 0.01$ versus 0.5 chance level, one-sample signed-rank test. (**H**) Similar to (G), but in the passive group ($n = 12$). $^{**}P = 0.003$ for 100% contrast. (**I**) Similar to (G), but in the anesthetized group ($n = 7$). $^{*}P = 0.031$ and 0.016 for 20 and 100% contrast, respectively. Holm $\#P < 0.05$ versus 0.5 chance level.

averaging the vectors of all trials except for a test trial. To decode the stimulus orientation, the vector in the test trial was compared with the centroids calculated at the same contrast as that in the test trial (contrast-matched condition). The decoding accuracy of each iteration was assessed by the probability of correct classification across all trials, and the decoding accuracies were lastly averaged across iterations. We found that the decoder accuracies in correct trials during task performance were significantly higher than those during passive viewing or under anesthesia at any contrast (Fig. 6B). This trend was also observed in the decoder formed using only responsive neurons (fig. S9A), individual rats (fig. S9B), or any bin size of analysis time window (fig. S9C). The decoder accuracy monotonically became higher as the number of neurons used for decoding in the task group was increased (fig. S9D, left). The decoder accuracy by only one neuron was still above the chance level in the task group after removing 11 neurons in descending order of the contribution to the accuracy (fig. S9D, right). In the passive and anesthetized groups, even after only one or two neurons were removed, the decoder accuracy for low-contrast stimuli fell to near the chance level (fig. S9, E and F, right). These results suggest that orientation information is sufficiently represented by even a relatively small number of neurons during task performance after training (*38*, *39*).

The distance between two orientation centroids was the farthest in the task group among three groups of rats at any contrast (fig. S10A), corresponding to the decoder accuracy (Fig. 6B). The variance in the task group was intermediate among the three groups (fig. S10B). Therefore, the separated representations of the two orientations seemed important for determining the decoder accuracy.

We next examined whether population activities relate to the behavioral choices in orientation discrimination using 20% contrast stimuli. Unlike the orientation representation at the single-neuron level (fig. S8B), the decoder accuracy at the population level was significantly higher in correct trials than in incorrect trials (Fig. 6C). To further quantify the relation between the decoder accuracies and behavioral choices, we projected the vector in the test trial on the discrimination axis connecting vertical and horizontal centroids and calculated the normalized distance between the centroid for the vertical stimuli and the projected vector (Fig. 6D). In correct trials, the normalized distances in vertical- and horizontal-orientation trials were well separated. However, in incorrect trials, these distributions substantially overlapped. The distances of the vertical or horizontal stimulation in correct trials were significantly different from those in incorrect trials. Thus, it is highly possible that the decoder accuracy is associated with the behavioral choices.

To evaluate the contribution of low contrast–preferring neurons to the decoder accuracy, we examined the effect of excluding low or high contrast–preferring enhanced-type neurons on population coding while keeping the total number of neurons in the population the same (Fig. 6, E and F). The accuracy of the decoder without the low contrast–preferring neurons significantly decreased at 20% contrast compared to that including these neurons, although it did not significantly change at 40 and 100% contrasts (Fig. 6E). The decoder accuracy without the high contrast–preferring neurons, resulting in higher proportion of the low contrast–preferring neurons in the population, significantly increased at 20% contrast, but did not significantly change at 40 and 100% contrasts (Fig. 6F). These results suggest that low contrast–preferring neurons contribute more considerably to the population representations of low-contrast orientation information than high contrast–preferring neurons.

Decoder analysis was so far performed under contrast-matched conditions between test trials and decoder calculations. We asked whether the population representations of orientation are common across stimulus contrasts or not. As a contrast-unmatched condition, the orientation in a test trial at 20% contrast was decoded by a decoder calculated using spiking activities in the 100% contrast trials and vice versa. The decoder accuracies in the test trials at both 20 and 100% contrasts were significantly lower in the contrast-unmatched than the contrast-matched condition in the task group (Fig. 6G). Thus, the population representations for stimulus orientation depended on stimulus contrast (*21*). As in the task group, in the passive and anesthetized groups, the decoder accuracy in the test trials at 100% contrast was significantly lower in the contrast-unmatched than the contrast-matched condition (Fig. 6, H and I). However, the decoder accuracy in the 20% contrast test trials was not significantly different between contrast-unmatched and contrast-matched conditions in the passive group. In the anesthetized group, it was slightly but significantly higher in the contrast-unmatched than in the contrast-matched condition. These results suggest that population activity is not specifically organized to represent low-contrast orientation information before training or under anesthesia, unlike during task performance after training.

Characterization and possible mechanisms of low-contrast preference

To determine the neuronal mechanisms of low-contrast preference, clarifying the dynamic activities of single neurons and local networks in each stimulus contrast is essential. To approach this, we first characterized the strength of spiking activity in significantly low and high contrast–preferring enhanced-type neurons in the task group (Fig. 7, A and B). Unexpectedly, in both WS and NS neurons, the spontaneous and cue-evoked activities (basal activities) were considerably higher in low than in high contrast–preferring neurons (Fig. 7A). High basal activities in low contrast–preferring neurons might be caused by high excitability. If so, then the visual responses could be also large even if visual inputs are small at low contrast (*40*, *41*). As expected, the firing rates during the 20% contrast stimulation were higher in low than in high contrast–preferring neurons (Fig. 7B). Responses to the respective preferred-contrast stimuli were also higher in low than in high contrast–preferring neurons (Fig. 7B). In significantly high contrast–preferring enhanced-type WS neurons, the spontaneous and cue-evoked firing rates were similar among the task, passive, and anesthetized groups (Fig. 7C). In NS neurons, these firing rates were similar between the task and passive groups but decreased during anesthesia (Fig. 7C). In both WS and NS neurons, the firing rates during the 20 or 100% contrast stimuli in significantly high contrast–preferring neurons were also similar among the three groups, except for NS neurons during anesthesia (Fig. 7D). Together, it was suggested that the increase in visual responses (Fig. 7, B and D) was accompanied with high basal activities (Fig. 7, A and C) in low contrast–preferring neurons that were preferentially observed during the task.

Training may also enhance bottom-up visual inputs. To examine this, we analyzed local field potentials (LFPs) recorded at the same time as spikes. The initial magnitude of visually evoked LFPs [visually evoked potentials (VEPs)] was larger in the task group than in the passive group at all the contrasts (Fig. 8, A and B). The

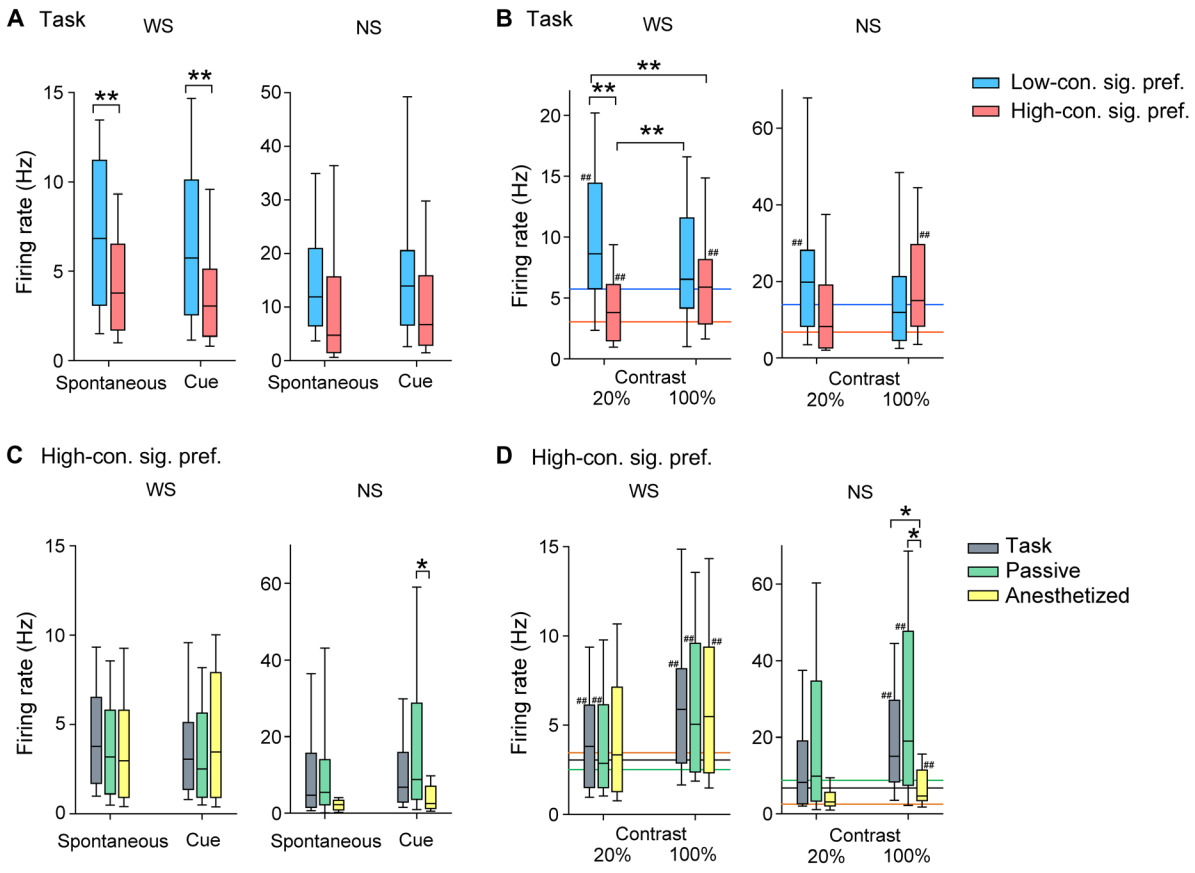

Fig. 7. Firing rates before and during visual stimulation. (**A** and **B**) Box plot summary of the firing rates in significantly low contrast–preferring ($P < 0.05$, Wilcoxon rank sum test) and high contrast–preferring enhanced-type neurons ($P < 0.05$) in the task group. The number of neurons was the same as that shown in Fig. 5A. (A) Firing rates during black (spontaneous) or gray display (cue). Holm-corrected $^{**}P < 0.01$, Wilcoxon rank sum test. (B) Firing rates during visual stimulation at 20 or 100% contrast. Holm $^{**}P < 0.01$, Wilcoxon rank sum test. Blue and red horizontal lines show the medians of firing rates during gray-cue display in low and high contrast–preferring neurons, respectively. Holm $\#\#P < 0.01$ versus cue, Wilcoxon signed-rank test. (**C** and **D**) Comparison of the firing rates of significantly high contrast–preferring enhanced-type neurons ($P < 0.05$) among the task, passive, and anesthetized groups. The number of neurons was the same as that shown in Fig. 5D. (C) Firing rates during black or gray-cue display. In NS neurons, the firing rates of the anesthetized group tended to be lower than those of the other two groups [cue: $P = 0.051$ versus task and $^{*}P = 0.034$ versus passive, Dunn's test after confirming significant difference by Kruskal-Wallis test (Holm $P < 0.05$)]. (D) Firing rates during visual stimulation. In NS neurons, the firing rates of the anesthetized group were significantly lower than those of the other two groups [20%: $P = 0.059$ versus task and $P = 0.055$ versus passive; 100%: $^{*}P = 0.014$ versus task and $^{*}P = 0.020$ versus passive, Dunn's test after Kruskal-Wallis test (Holm $P < 0.05$)]. Colored lines indicate the median firing rates during cue in (C). Holm $\#\#P < 0.01$ versus cue, Wilcoxon signed-rank test.

potentiation of bottom-up inputs seems to contribute to driving V1 neurons even when the stimulus contrast is low.

Here, although the $F1/F0$ ratio for the linearity of response to drifting stimuli, which was calculated using the responses at preferred contrast, was similar between significantly low and high contrast–preferring enhanced-type neurons (fig. S3B), the contrast dependence of $F1$ (the modulated component at the stimulus frequency) directly relating to bottom-up inputs was generally different between significantly low and high contrast–preferring neurons (fig. S11A). In high contrast–preferring neurons, $F1$ was larger at high contrast than at low contrast. On the other hand, in low contrast–preferring neurons, the contrast dependence of $F1$ was diverse without one-directional trend, and $F1$ was not significantly different between high and low contrast. On the contrary, $F0$ (the mean response) was large at the preferred contrast in both low and high contrast–preferring neurons (fig. S11B). Therefore, $F0$, an additive constant, would be important especially for large responses at low contrast in low contrast–preferring neurons. It might be related to top-down inputs that depend on contrast, rather than bottom-up inputs.

Furthermore, to explore contrast-dependent changes in LFPs after training, we analyzed the time-frequency spectrogram of the LFPs. Various frequency oscillations were observed (Fig. 8, C and D, and fig. S12, A and B). In particular, the beta oscillation (18 to 30 Hz) was more strongly induced by grating stimulation at 100% contrast than it was at 20 or 40% contrast (Fig. 8, C and D). The beta oscillation during the 100% contrast grating was significantly larger than without visual stimulation (dark) in the task and passive groups (Fig. 8E). This beta oscillation was more strongly observed in the task group than in the passive group (Fig. 8E). In the task group, the magnitude of the beta oscillation was not affected by movements (fig. S12, C to E). We also evaluated the degree of the phase synchronization of spikes to the LFP using the spike-LFP pairwise phase consistency (PPC), which can rule out the differences in spike

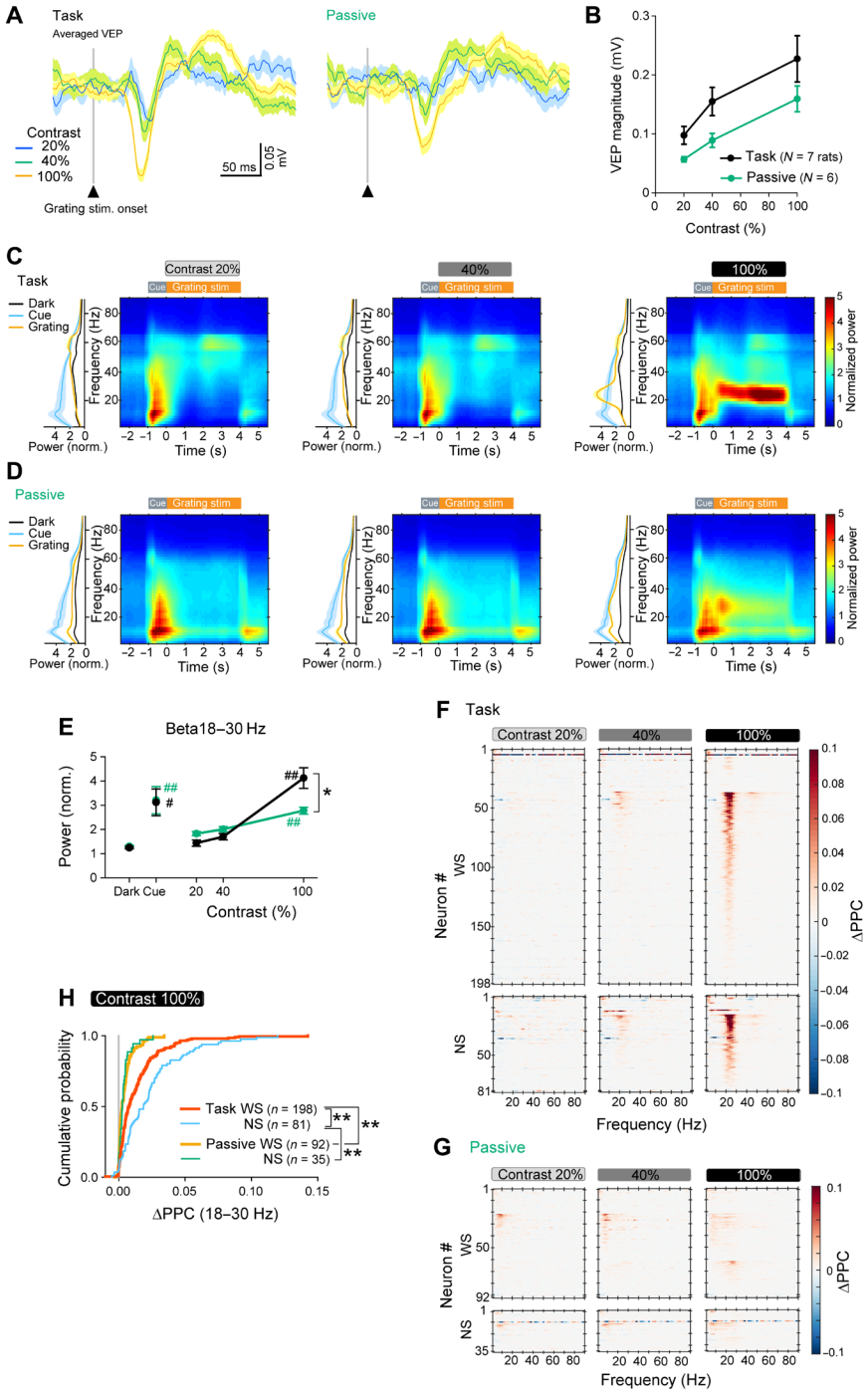

Fig. 8. Changes in LFPs and their coupling with spikes after training. (**A** and **B**) Comparison of visually evoked LFPs (VEPs) between the task and passive groups. (A) Examples of trial-averaged VEPs in a session (shaded area, SEM). (B) Averaged VEP magnitudes in the task ($N = 7$ rats) and passive groups ($N = 6$). (**C** and **D**) Color map, averaged LFP time-frequency spectrogram during grating stimulation at each contrast, which was normalized using the mean power across all frequency bands (1 to 90 Hz) for 0.5 to 1.5 s before the cue onset. Line graph, the time-averaged power spectrum (shaded area, SEM) in the respective periods (dark, −2.5 to −1.5 s from the grating onset; cue, −1 to 0 s; grating, 0 to 4 s). (C) Task ($N = 7$). (D) Passive ($N = 6$). (**E**) The magnitude of the beta oscillation (18 to 30 Hz) in the above-described periods. The beta oscillations were significantly larger during cue and grating stimulation at 100% contrast than during dark condition [task, cue, #$P = 0.021$; 100% contrast, ##$P < 0.001$, Dunn's test after confirming significant difference by Kruskal-Wallis test ($P < 0.001$); passive, cue and 100% contrast, ##$P < 0.001$, Dunn's test after Kruskal-Wallis test ($P < 0.001$)]. The beta oscillation at 100% contrast was significantly stronger in the task group than the passive group (*$P = 0.035$, Wilcoxon rank sum test). (**F** and **G**) The spike-LFP PPC during gratings at each contrast in the task (F) (WS, $n = 198$; NS, $n = 81$) and passive groups (G) (WS, $n = 92$; NS, $n = 35$). Individual ΔPPCs (baseline-subtracted PPCs) during gratings were pseudo-colored and sorted in descending order according to the ΔPPC values in each preferred band (theta, 1 to 4 Hz; alpha, 6 to 16 Hz; beta, 18 to 30 Hz; gamma, 40 to 70 Hz). (**H**) Cumulative distributions of ΔPPCs in the beta band (18 to 30 Hz) at 100% contrast in WS and NS neurons in the task and passive groups. Holm-corrected **$P < 0.01$, Kolmogorov-Smirnov test.

rates (Fig. 8, F and G) (*42*). In the task group, spikes in both WS and NS neurons were strongly synchronized to the beta band oscillations during the 100% contrast stimuli (Fig. 8F). This spike-LFP synchronization in the beta band did not occur in the passive group (Fig. 8G). Furthermore, we found that this synchronization was significantly stronger in NS than in WS neurons of the task group (Fig. 8H). It has been reported that synchronized activities have a stronger impact on network activities (*43*). Thus, our results suggest that the inhibition is more enhanced than the excitation in the presence of high-contrast stimuli after training. Changes in the excitatory-inhibitory balance during high-contrast stimuli may lead to low-contrast preference.

We next compared the strength of phase synchronization during the 100% contrast visual stimulation between low and high contrast–preferring enhanced-type neurons in the task group. It has been reported that phase-locked activities are possibly more interactive (*43*, *44*). Thus, if low contrast–preferring WS neurons show strong phase synchronization together with the NS neurons in the presence of high-contrast stimuli, then the WS neurons can receive relatively strong inhibition. However, phase synchronization was not significantly different between low and high contrast–preferring neurons in both WS and NS neurons (fig. S13, A and B). We also analyzed the preferred phase. All neuron types tended to fire preferentially at approximately the trough of beta oscillations during high-contrast stimulation. However, the preferred phase of low contrast–preferring WS neurons was similar to that of the NS neurons with low- or high-contrast preference (fig. S13C). In contrast, the preferred phase of high contrast–preferring WS neurons was significantly different from that of low or high contrast–preferring NS neurons (fig. S13C). Because of the similar trough preference between NS neurons and low contrast–preferring WS neurons, low contrast–preferring WS neurons may be more affected by the inhibition during high-contrast stimulation than high contrast–preferring WS neurons, resulting in a decrease in responses to high-contrast stimuli. Although this modulation, of course, must be affected by the difference of firing rates between low and high contrast–preferring NS neurons, the firing rates at high contrast were not significantly different between those NS neurons (Fig. 7B). Therefore, NS neurons would work for the inhibition in beta oscillations, irrespectively of contrast preference.

DISCUSSION

We show that low-contrast preference is strengthened during an orientation discrimination task after iterative training irrespective of functional neuronal subtypes in the deep layers of rat V1. Low contrast–preferring neurons represent orientation information with low contrast more accurately than high contrast–preferring neurons. Many previous reports have demonstrated that visual cortical neurons typically exhibit a monotonic saturating increase in visual responses as the stimulus contrast increases in both anesthetized and awake conditions (*13*–*16*). Other than these responses, some previous studies have reported the responses with specific-contrast preference in monkey V1/V2 and V4 (*17*, *18*) and mouse V1 (*19*–*22*). Even before learning, low-contrast preference was recently reported to be observed more in layer 2/3 than in deep layers where we recorded (*22*). We found that the low contrast–preferring enhanced-type responses are related to the accuracy of visual discrimination after learning. Here, we classified the neurons showing enhanced (above basal activities)–type visual responses at preferred contrast differently from the neurons showing only depressed (below basal activities)–type responses. Considering information representation, these two types of neurons would function quite differently (*27*). Low contrast–preferring responses include both enhanced-type and depressed-type ones. However, in this research, we especially focused on enhanced-type ones and revealed the functional importance of low contrast–preferring enhanced-type responses.

It was previously reported that contrast gain increases in cat V1 after learning (*12*). In our study, a subset of enhanced-type neurons was tuned to low contrast rather than simply increasing the contrast gain. As low-contrast preference was strengthened specifically in the task group after training, learning-dependent plastic changes in neuronal circuits and/or the effects of top-down controls or brain states seem to be involved in the establishment of low-contrast preference.

Low contrast–preferring enhanced-type neurons showed high basal activities after training, which indicates that membrane excitability and/or spontaneous depolarization is high in these neurons. We also observed large bottom-up inputs irrespective of stimulus contrasts following training, being involved in evoking strong responses. Furthermore, repetitive activation is known to build neuronal ensembles by strengthening recurrent excitatory synapses between coactive neurons following Hebb's rule (*45*). These enhanced excitations are likely to contribute to increasing visual responses even when visual contrast is low (*40*, *41*).

The enhanced excitation can also increase the responses to high-contrast stimuli. However, the responses to high-contrast stimuli were similar before and after learning. Thus, inhibition may suppress visual responses to high-contrast stimuli after learning. Strong beta oscillations were observed specifically during high-contrast stimulation following training. The phase synchronization of spikes to the beta oscillations was stronger in putative inhibitory neurons than excitatory neurons. Phase-locked activities with temporal precision have a great impact of the net activity (*43*, *46*). Moreover, rhythmic inhibition modulates firing rates in a phase-dependent manner (*44*, *47*). In addition, stabilized supralinear network models that currently mainly consider firing rates are known to also provide a simple account of contrast-dependent response (*48*). As external stimulus strength grows, the modeled system moves into an inhibition-stabilized network (ISN) regime (*22*, *48*, *49*). Furthermore, it is quite likely that plastic changes during learning, such as strengthened recurrent excitation, more certainly switch from the non-ISN regime toward the ISN regime, causing strong inhibition at high contrast. After learning, we also observed the increase of low contrast–preferring inhibitory neurons showing sufficient activities even at high contrast. Together, inhibition can more strongly act during high-contrast than low-contrast stimuli. Considering the generally enhanced excitation and the larger inhibition during high-contrast stimuli, the responses to low-contrast stimuli can be larger than those to high-contrast stimuli in some cases. Here, the beta oscillations are preferentially driven by somatostatin (SOM)–expressing interneurons (*50*). The SOM interneurons show relatively strong responses to high-contrast stimuli via a mutually antagonistic relationship with low contrast–preferring vasoactive intestinal peptide (VIP)–expressing interneurons (*22*). Together, the beta oscillations may occur specifically during high-contrast stimulation. Our result of the strong inhibition in high-contrast stimuli may be reminiscent of previous findings that visual responses in V1 neurons are suppressed by large stimuli (*51*), particularly at high

contrast (*52*). Surround suppression is reported even under anesthesia, although it is attenuated compared to the awake state (*53*). Because we did not observe low-contrast preference of enhanced-type activities in anesthetized rats after training, the contribution of this surround suppression may be limited.

Low-contrast preference of enhanced-type activities detected during task performance disappeared following anesthesia. The top-down inputs from the higher cortical areas have been shown to remarkably decrease under anesthesia (*54*, *55*). The top-down control and cholinergic modulation originating from the basal forebrain are active during high attention (*56*), for example, task performance. In addition, these nonsensory inputs modulate neuronal activities in V1 (*10*, *43*, *57*–*59*). Thus, these nonsensory signals are likely involved in low-contrast preference. This is also supported by our result that an additive constant ($F0$) was important for low-contrast preference in enhanced-type activity. The top-down inputs have been reported to increase sensory acuity (*9*, *60*). For example, cingulate cortex activation can improve the orientation representations in V1 neurons and visual perception (*23*). In addition, cholinergic inputs improve representations of visual information in V1 (*61*) and visual perception (*24*). Because response strength in low contrast–preferring neurons was correlated with task performance, the top-down and/or cholinergic modulation may preferentially affect the activities in low contrast–preferring neurons. Multiple mechanisms may be involved in the generation of low-contrast preference. The findings of this paper would be meaningful to provide the experimental data for understanding neuronal mechanisms underlying visual perception for low-contrast stimulation. Further studies are needed to clarify the mechanisms, for example, by characterizing inputs to the low contrast–preferring neurons.

Our results showed that orientation discriminability for low-contrast stimuli in single low contrast–preferring enhanced-type neurons in the task group after training was better than that in high contrast–preferring neurons observed before and after training. In contrast, the discriminability for high-contrast stimuli did not differ between low and high contrast–preferring WS/NS neurons during the task or between before and after training for WS neurons. Thus, at the single-neuron level, orientation discriminability seems to be improved after training but, in excitatory neurons, preferentially when the visual contrast was low. On the other hand, at the population level, the training improved the decoding accuracy at all the contrasts. This evidence suggests that low-contrast orientation information is well represented in both single-neuron and ensemble activities of newly recruited neurons with low-contrast preference after training, while the representation of high-contrast orientation information is improved preferentially in ensemble activities. In addition, orientation representation would be more stable at the population level than at the single-neuron level, directly connecting with task performance.

Although the orientation tuning in cat is contrast invariant (*16*), in rodents, orientation tuning in excitatory neurons is sharpened upon an increase in stimulus contrast (*62*, *63*). Also in our results, high contrast–preferring enhanced-type neurons showed contrast-dependent increases in orientation discriminability. On the other hand, low contrast–preferring enhanced-type neurons displayed contrast invariance. A recent simulation study (*62*) revealed that strong inhibition and orientation-preferential excitation could generate the contrast dependency. The excitatory-inhibitory balance as stated above is thought to affect the contrast dependency of orientation discriminability.

Our analysis, using contrast-matched and contrast-unmatched decoders, showed that the orientation information at each contrast after training was represented in a different ensemble activity (*21*). High-contrast orientation information was expressed in the ensemble activity of both low and high contrast–preferring enhanced-type neurons, as shown by the effect of excluding either contrast-preferring neurons on the decoder accuracy. We also found that the number of visual responsive neurons assessed using the vertical- and horizontal-orientation stimulation had increased after training. These results suggest that the representation of the two orientations is redundant (*64*) after training. The decoding accuracy for orientations almost monotonically decreased with the reducing number of neurons in descending order of the contribution to the accuracy, indicating that the orientation information was distributed across multiple neurons (*36*). This suggests that the redundancy in excessive neurons functions to represent repeatedly experienced orientations irrespective of contrast. Particularly, the neuronal activities processing low-contrast visual information were newly established after training. This experience-dependent change in information representation may stabilize the behavioral performance of visual discrimination in a natural visual environment.

MATERIALS AND METHODS

Animals

All procedures were approved by the Animal Care Committee of the National Institutes of Natural Sciences and performed in accordance with its guidelines. Adult male Long-Evans rats (Institute for Animal Reproduction; 9 to 11 weeks old, 348 ± 8 g at the time of surgery; N = 14 rats) were kept under an inverted light schedule (12 hours:12 hours).

Surgery

Rats were subjected to surgery before starting behavioral training. Anesthesia with isoflurane was induced at 5.0% and maintained at 2.0 to 2.5% (v/v; Univentor 400 anesthesia unit, Univentor, or MK-A110D, Muromachi) (*65*, *66*). During anesthesia, body temperature was maintained at 37°C using a heating pad (BWT-100A, Bio Research Center). If necessary, we used additional surface anesthetic (lidocaine hydrochloride) for head skin incision and ophthalmic lubricant ointment to prevent eye dryness. Teflon-coated silver wires (200 μm in diameter; A-M Systems) were implanted for reference and grounding above the cerebellum. Antibiotics and/or anti-inflammatory drugs were locally applied [0.4% aminoglycosides amikacin in saline or phosphate-buffered saline (PBS) and/or 0.3% steroidal prednisolone ointment including antibiotic chloramphenicol and fradiomycin] as required after surgery. A sliding aluminum head attachment (CFR-1, Narishige) was surgically attached to the skull with tiny anchor screws (stainless steel, 1 mm in diameter, 2 mm long), dental resin cement (Panavia F2.0, Kuraray Medical), and resin (UNIFAST II, GC Corporation). The skull was additionally guarded by dental resin cement (BISTITE II, Tokuyama Dental, or Super-Bond C&B, Sun Medical) and silicone sealant (Dent Silicone-V, Regular, Shofu). Rats were allowed 6 to 11 days of recovery before undergoing water restriction for behavioral training.

One or 2 days before the beginning of the electrophysiological recording, the rats were subjected to a second surgery under anesthesia, which was maintained with about 1.5 to 2.5% isoflurane. A tiny hole

(about 1 mm in diameter) was opened in the skull, and the dura mater was beforehand removed for silicon probe insertion. The hole was above the monocular region of the left V1 (7.0 ± 0.5 mm posterior, 3.5 ± 0.5 mm lateral from bregma). When the rats were not undergoing electrophysiological recording, the hole was covered by a silicone sealant (Dent Silicone-V).

Orientation discrimination task

Head-restrained rats were placed in a cylinder (a body restrainer) of the operant chamber before starting electrophysiological recordings. The chamber contained an improved version of the spout lever that integrated the lever and reward into one device (*65*). In this new version, the lever moved in conjunction with the spout but was separated so that rats could push and pull it with their right forelimb evenly and easily ($P > 0.05$, comparison of correct ratios between push and pull at each contrast, Wilcoxon signed-rank test, $N = 7$ rats; Fig. 1C). The spout lever was horizontally movable in the forward (by push, up to 0%) and backward (by pull, up to 100%) directions. The holding position of the lever to start the task was defined as 30 to 70% of the movable range. The task started when rats held the lever in the holding position for 0.5 s (Fig. 1A). At the start of the task, a gray cue was presented for 1 s, followed by drifting gratings of vertical or horizontal orientation at 20, 40, or 100% contrast for 4 s. Rats had to respond to vertical gratings by pushing the lever and to horizontal gratings by pulling it. Push and pull positions were defined as 0 to 30% and 70 to 100% of the movable range, respectively. The rats had to hold the lever in the appropriate position for at least 0.5 s within 1 to 4 s after the grating onset to acquire a drop of 0.1% saccharin water (0.015 ml; saccharin sodium dihydrate). The reward was applied 0.1 to 0.5 s after judgments of the appropriate movement. In the case of incorrect movements (duration, 0.5 s), rats were not punished, and there was no repetition of the same gratings as in the incorrect trials, different from the training periods (see below). Intertrial interval (ITI) was set to 6 to 10 s at random, and a black screen was displayed during the ITI. The lever trajectory was always detected by an angle encoder (MES-12-1000 PC, Microtech Laboratory). Especially for recording sessions, an arm rest bar for the right forelimb was removed. For this reason, the rats, which were calm in a cylinder in a familiar environment, held the lever with their right forelimb most of the time to stabilize their postures. The lever trajectory was considered to reflect the amount of behavior. The task-related event logs (e.g., ITI onset, judgment time, and reward onset) were recorded on the same recorder as for electrophysiological recordings (32-channel hard-disk recorder, LX-110F, TZ-LXSY2 for synchronous recordings, TEAC). During the experiments, white noise (64 dB) was broadcasted to prevent accidental external noises that could disturb the task performance or affect neuronal activities. The task was performed in a session (about 700 trials, for 2 to 3 hours; fig. S1B) per day.

Rats were deprived of water in their home cage and were provided with the minimum necessary amount of water as a reward during task performance. When rats did not participate in the task or when the amount of reward that they received was small, an agar block containing water was given (*65*, *66*). Food was available ad libitum.

Behavioral training

Rats were familiarized with a cylinder (hideaway) in their home cage, and each rat was briefly (10 min) handled once a day for 2 days. Before the start of training on the abovementioned orientation discrimination task, drinking water was restricted under careful observation. An agar block including water was applied per day for the first 3 days, and then water was deprived for 2 days.

In the first phase (4 to 9 days), rats were required to keep the lever in the holding position for 0.1 s and move it in response to the 100% contrast visual stimulation presented. Rats were trained to respond to a vertical grating by pushing the lever and to a horizontal grating by pulling it to acquire a drop of saccharin water. The vertical- and horizontal-grating blocks (20 to 100 trials in each block) were alternated. During this phase for some rats, we intervened in the training by helping rats to operate the lever. Later, in this phase, rats were required to keep the lever in the holding position for 0.5 s to start the task. Rats were trained to move the lever to the push/pull position depending on the stimulus orientation and maintain the position for at least 0.5 s. The reward was supplied 0.1 to 0.5 s (at random) after the judgment of the correct movement. In the case of incorrect movements (duration, 0.3 s), rats were punished by a mild air puff (0.5-s duration, 0.1- to 0.3-s delay at random) toward the base of the neck. Once rats could perform the specific movements in response to the stimulation, rats were advanced to the second phase.

In the second phase (11 to 35 days; 23.1 ± 3.6 days; $N = 7$ rats), the 100% contrast vertical and horizontal gratings were pseudo-randomly interleaved at a 1:1 ratio. Early in this phase, when rats performed an incorrect movement (duration, 0.3 s), they were punished by a mild air puff and were required to reperform the same orientation trial until the movement was correct (correction trials). In some cases, during this phase for the first several days, we also intervened in the training by helping rats to operate the lever. Later, this punishment continued but the correction trials stopped. The rats were judged as passing this phase by achieving an 85% correct ratio (= correct trials / [correct trials + error trials] × 100) on two consecutive days. In addition, rats were trained to stay for about 1 hour in the recording chamber, because this period was necessary for later electrophysiological recordings (stabilization of the inserted electrode).

After the training sessions, 20 and 40% contrast stimuli were added. To avoid confusing rats by difficult discrimination, more trials at 100% contrast were included (*67*). The ratio of 20, 40, and 100% contrast was 1:1:2. The rats were determined to pass this phase when the correct ratio of orientation discrimination including lower contrasts was about 80% on three consecutive days.

In the passive group, rats were water-restricted and habituated to the head-restrained condition and recording chamber for three sessions (2 to 3 hours of session per day), similar to the task group. During this habituation period, a gray screen was displayed, and rats were pseudo-randomly given the reward. During the second and third sessions, rats were also trained to stay for about 1 hour, as needed for later recordings.

Visual stimulation

Visual stimuli were generated with a PC equipped with an NVIDIA GeForce GTX780 (3 GB) graphics board and MATLAB (MathWorks) using the Psychophysics Toolbox extensions (Psychtoolbox-3; http://psychtoolbox.org/) (*68*, *69*). The stimuli were presented on a 23.0-inch thin-film transistor monitor [in-plane–switching, liquid crystal display, light-emitting diode backlight; FORIS FS2333-A, EIZO; 510 mm by 287 mm, 1920 × 1080 pixels, 60-Hz refresh rate, 230 to 240 cd/m^2 maximum luminance; cf. (*24*, *25*)] and were gamma-corrected with

custom software and a luminance meter (LS-100, Konica Minolta). The monitor was located 23 cm from the right eye (contralateral eye to the recording hemisphere) and positioned to present visual stimuli covering the receptive fields of the recorded neurons. The receptive fields were estimated by manually moving the white bar on the black display.

Visual stimuli consisted of full-field sinusoidal gratings of vertical (from right to left, i.e., back-to-front motion) or horizontal orientation (from bottom to top) at 20, 40, or 100% contrast (spatial frequency, 0.04 cycles/deg) drifting at a temporal frequency of 2 Hz. The orientation and contrast were pseudo-randomly selected. The same orientation was set so as not to continue more than twice. The ratio of vertical and horizontal orientations was 1:1. The ratio of 20, 40, and 100% contrast was 1:1:2, as stated above. The actual trial number per session for each orientation or each contrast corresponded to these ratios in the task group (351 ± 14 trials for vertical grating and 351 ± 14 for horizontal; 88 ± 4 for the 20% contrast vertical/horizontal stimuli, 88 ± 4 for 40%, and 176 ± 7 for 100%; $N = 7$ rats). The gratings were presented for 4 s after the 1-s gray-cue screen with the same mean luminance as that of the gratings. The visual stimuli were triggered by the task system (O'Hara & Co) and presented using custom codes of the Psychophysics Toolbox. To measure the precise onset time of visual stimuli, a white or black small rectangle, which was displayed in the upper left corner of the monitor at the time of the visual stimulus onset, was detected by the photosensor (O'Hara & Co). Common visual stimuli were used for electrophysiological recordings in the task, passive, and anesthetized groups.

Electrophysiological recordings

We performed extracellular multiple single-unit recordings from the monocular region of V1. A 16-channel silicon probe (A2x2-tet-3mm-150-150-121, NeuroNexus; two shanks with two tetrode-like sites per shank at 150-μm intervals, 15-μm thickness, 121 μm^2 each site, 0.5- to 2-megohm impedance) was placed on the brain surface in the skull hole, and then the hole was covered with 2% agarose (Agarose-HGT, Nacalai Tesque; in PBS). After that, the probe was inserted vertically into the putative layer 5 of the left V1 (7.0 ± 0.5 mm posterior, 3.5 ± 0.5 mm lateral from bregma, 1.1 ± 0.2 mm deep; fig. S1C) using a micromanipulator (SM-25A, Narishige) on a stereotaxic frame (SR-10R-HT, Narishige). The agarose-covered hole for the insertion was additionally covered with paraffin wax (granular and liquid paraffin mixed in a 1:1 ratio) to prevent drying. After more than 1 hour of stabilization, the electrophysiological recording was started. Multichannel signals were amplified (final gain, 1000; original band-pass filter, 1 to 5 kHz; preamplifier, μPA16; amplifier, PGA-32; adapter, ADPT-NN-A16-μPA16, Multi Channel Systems) and digitized by 32-channel hard-disk recorders (sampling, 20 kHz; LX-110F).

In the task and passive groups, the recording was conducted in one session (one penetration) a day and repeated for 3 to 7 days. To prevent infections during repetitive recordings, antibiotics and anti-inflammatory drugs were locally applied after the recording, such as during the surgery.

In the passive group, the trial was started when rats held the lever around the center position. Rats in the passive group were given water pseudo-randomly in 50% of the trials during a black ITI screen within 1 to 5 s after the end of gratings. The total ITI period was set to 8 to 12 s and was of similar length to that in the task group, but a little longer because of securing the drinking time.

Some rats in the task group were anesthetized with urethane [25% aqueous solutions; 5 ml kg^{-1} intraperitoneally (i.p.), further injected when necessary] on the last recording day. In the anesthetized group, the recording was performed in one to three sessions within the day. The right eyelid was stretched with silk threads under additional local anesthesia (1% xylocaine injection with epinephrine, subcutaneously; AstraZeneca) to open the visually stimulated eye, and the eye was covered with transparent dimethyl silicone oil (KF-96H-6,000 centistokes, Shin-Etsu Chemical) after applying the saline to prevent drying. During anesthesia, the body temperature was maintained at 37°C using a heating pad.

During electrophysiological recordings, the behavior and left eye (unstimulated eye) of the rats were monitored by an infrared monochromatic charged-coupled device video camera (type 323, O'Hara & Co) and recorded at 29.97 frames/s, along with the display for visual stimulation. On the basis of the eye image, trials with closed eyelids were eliminated from the analyzed data in the passive group. In the task group, rats usually opened their eyelids in correct and incorrect trials. In the anesthetized group, the eye was forced to open with the threads, as stated above.

To check electrode positions, the rats were placed under deep anesthesia with urethane (25% aqueous solutions; 7 to 10 ml kg^{-1} i.p.) and intracardially perfused with cold saline followed by 4% paraformaldehyde. The brains were postfixed and sliced coronally into 50-μm-thick serial sections using a microslicer. The sections were examined using a BZ-X700 all-in-one microscope (KEYENCE).

Quantification and statistical analysis

Spike extraction and refinement

Multiple single-unit recording data were processed offline to isolate spike events, using the automatic spike-sorting program EToS (Efficient Technology of Spike-sorting; http://etos.sourceforge.net/) (*70*, *71*). A high-pass filter was designed to subtract Gaussian smoothed signals ($\sigma = 0.25$ ms) from the raw signals. For a high-pass–filtered signal (x), the negative peak below the threshold (median$[x] - 5 \times$ SD$[x]$; where SD, a robustly estimated SD, SD$[x]$ = median$[|x - \text{median}[x]|]/0.6745$) was detected as a spike candidate. Only one spike candidate could be detected within a time window of 0.5 ms to avoid repeatedly detecting the same spike. The wavelet transform was applied to the waveforms of spike candidates. The features of the spike candidates were extracted using multimodality-weighted principal components analysis on the wavelet coefficients. Then, spike candidates were automatically clustered by explicit variational Bayes for Student's t mixture model of the extracted features. In both feature extraction and clustering, the dimension per channel was set to 3. After that, the sorted spike clusters were manually combined, divided, or discarded to refine single-neuron clusters, based on the absence or presence of refractory periods (<2 ms) in their own autocorrelograms (ACGs; related to interspike interval) and cross-correlograms (CCGs) with other clusters, using a cluster cutting application (Klusters) and a viewer (Neuroscope) (http://neurosuite.sourceforge.net/) (*72*). If a CCG of two clusters isolated from different tetrodes exhibited a sharp peak just in the 0-ms bin, followed by a refractory period, then the two clusters were considered to come from the same neuron. In that case, we excluded the smaller-size cluster. We confirmed that the final form of each cluster had a clean refractory period in its ACG and few refractory periods in its CCGs with the other clusters. We selected single-unit activities in which the total number of spikes

was ≥4000 (*66*) and the larger of the averaged spiking responses for the first 1 s during vertical or horizontal gratings across three contrasts (20, 40, and 100%) was ≥1 Hz. Then, we selected sessions in which the number of simultaneously isolated neurons was ≥4 for subsequent analysis.

Data analysis of single-unit activities

We analyzed multiple single-unit activities recorded during a period that included ≥20 preferred-orientation trials at respective contrasts with correct behavioral answers in the task group and with omissions (without lever movement–like answers) in the passive or anesthetized group. If a session included more than 25% incorrect trials at 100% contrast in either orientation in the task group, then all data from the session were discarded.

The averaged firing rates during the black display were assigned as spontaneous activity. In the case of supplying rewards (in the task and passive groups), the analysis window for this activity was from 2 s after the grating end or reward end (whichever was later) to 1 s before the cue onset in the next trial. In the case of no-reward trials (in the passive and anesthetized groups), the time window was from 2 s after the grating end to 1 s before the next cue onset. The firing rates for the second half (0.5 s) of the period during the gray cue were assigned as cue activity. The firing rates for the first 1 s during gratings before receiving rewards were basically defined as visual responses, thus avoiding the contribution of activities related to rewards (*73*). The preferred orientation was defined as the orientation (vertical or horizontal) that gives the largest magnitude of response for the first 1 s during gratings at the three contrasts (20, 40, and 100%). Visual responses to the preferred orientation were basically analyzed, unless the calculation of CIs and PIs for responses to the nonpreferred orientation (figs. S5 and S6, A to C).

Classification of neurons

WS and NS neurons. The distribution of spike durations from the trough to the peak was separated into two groups with a boundary of around 0.5 ms (fig. S1, D, F, and H). On the basis of this separation, neurons were classified as WS (spike duration ≥ 0.5 ms) and NS (<0.5 ms) neurons. WS and NS neurons were putative excitatory and inhibitory neurons, respectively (*66*, *74*).

Visual responsiveness. The absolute values of trial-averaged firing rates after subtracting the cue activity were calculated in individual neurons, for every 80-ms window (four consecutive 20-ms bins) during grating presentations (4 s) with every combination of orientations (vertical and horizontal) and contrasts (20, 40, and 100%). When the largest values of the firing rates exceeded two times the SD of the cue activity in all of the four 20-ms bins, the neurons were assigned to the visually responsive category.

Enhanced and depressed type. Among the visually responsive neurons, the neurons were regarded as "enhanced-type" or "depressed-type" when the magnitude of the visual responses, which were identified with a combination of orientations and contrasts as described above, was positive or negative after subtraction of the cue activities, respectively. If the neurons satisfied both criteria during the grating presentations, then the neurons were classified as the enhanced type.

Stimulus contrast selectivity of neuronal responses

To assess contrast preference in the visually responsive neurons, we calculated the CI as follows

$$\mathrm{CI}\,[R_{\mathrm{con100\%}}, R_{\mathrm{con20\%}}] = \frac{R_{\mathrm{con100\%}} - R_{\mathrm{con20\%}}}{R_{\mathrm{con100\%}} + R_{\mathrm{con20\%}}} \quad (1)$$

where $R_{\mathrm{con100\%}}$ and $R_{\mathrm{con20\%}}$ are the averaged firing rates for the first 1 s during the grating at 100 and 20% contrast, respectively. We confirmed that the results calculated by using the first 1-s and whole 4-s responses were almost the same (fig. S4G). For the analysis on effects of the lever movements (fig. S4D), the data were used that included more than eight trials (≥8) with and without lever movements at each of all tested contrasts.

On the basis of the CI values, the neurons were assigned as high contrast–preferring (CI ≥ 0.025) and low contrast–preferring neurons (CI ≤ −0.025). A single bin of around 0 in the histograms for the CIs (Fig. 3, A, C, and E) was removed for the classifications of high or low contrast–preferring neurons. In addition, the significance of the contrast preference of individual neurons was evaluated by comparing the spike numbers between the 100 and 20% contrast trials using Wilcoxon rank sum test ($P < 0.05$). Furthermore, we evaluated whether the significantly low contrast–preferring neurons significantly existed by bootstrap test. We resampled visual activities with an equal number of trials at 100 and 20% contrasts (the smaller number of trials was adopted) and randomly swapped the activities. The bootstrapped data were obtained by repeating these operations 10,000 times for each neuron. The *P* value was estimated as the probability that the number of low contrast–preferring neurons in shuffled bootstraps was the same or higher than that in real data. In addition, the significance of the preference at the neuronal population level was evaluated by one-sample Kolmogorov-Smirnov test of whether the CIs from real data were derived from the assumed distribution of CIs calculated using the shuffled bootstrapped data.

To examine an influence on the CI values by the variability of the responses, we resampled the neurons with the similar coefficient of variation (CV; CV = SD/average) to each other, allowing duplication. Specifically, we uniformized the CVs at 20% contrast between the task and passive groups (fig. S4I), because WS neurons had larger differences at 20% contrast than 100% (fig. S4H). We combined the data resampled from two directions as follows. After extracting both data from the overlapping range in the task and passive groups, one direction resamples the data in the passive group with the CV similar to that of the respective data in the task group. The other direction resamples the data in the task group with the CV similar to that of the respective data in the passive group. After this manipulation, we compared the CIs between the task and passive groups (fig. S4J).

Peristimulus time histograms

The PSTHs in individual neurons were calculated by averaging the activities aligned to the grating onset (bin width, 20 ms). For obtaining a global view of all PSTHs (Fig. 2, C and D), the histograms were calculated by averaging the activities aligned to the grating onset with a Gaussian filter (resolution, 0.5 ms; σ = 50 ms; length, 500.5 ms). These filtered PSTHs were then normalized by the highest responses to the preferred contrast (20, 40, or 100%; during whole grating stimulation period, 4 s) after subtracting the cue activities and pseudocolored. For averaging PSTHs (Fig. 2, E and F), the filtered and normalized PSTHs (as stated above, but the preferred contrast was 20 or 100%) were aligned to the peak time within 0.5 s from the grating onset, given the temporal frequency of 2 Hz, and then averaged.

Linearity of response to drifting gratings

The linearity of response was used for classifying V1 neurons into simple- and complex-response types (*15*, *20*). To calculate the linearity, the discrete Fourier transform was applied to the PSTHs of

the responses to the 4-s gratings with the preferred orientation and contrast after subtracting the cue activities. Then, the *F*1/*F*0 ratio of the modulated component (*F*1; at the stimulus frequency) to the mean response (*F*0) was computed (fig. S3B). In addition, the contrast dependency of the *F*1 and *F*0 were analyzed (fig. S11).

Characterization of firing patterns

Each ACG was filtered by a Gaussian filter (resolution, 0.05 ms; σ = 3 ms; length, 30.05 ms), normalized against the baseline period (150 to 250 ms), and pseudo-colored (fig. S3C) (*35*).

Selectivity of responses to correct/incorrect trials

The PI was calculated in trials with 20% contrast visual stimuli, including incorrect choices as follows

$$\mathrm{PI}\,[R_{\mathrm{correct}}, R_{\mathrm{error}}] = \frac{R_{\mathrm{correct}} - R_{\mathrm{error}}}{R_{\mathrm{correct}} + R_{\mathrm{error}}} \quad (2)$$

where R_{correct} and R_{error} are the averaged firing rates for the first 1 s during the grating in correct and incorrect trials. For selectivity between these trials, we analyzed the data containing more than 15 trials (≥15) in the respective correct and incorrect trials. The significance was tested in the same way as for CI, as stated above.

Discriminability between vertical and horizontal orientations in individual neurons using the d-prime

The *d*-prime (effect size; Cohen's *d*) was calculated as follows

$$d' = \frac{|R_{\mathrm{vertical}} - R_{\mathrm{horizontal}}|}{\text{pooled standard deviation}_{\text{vertical and horizontal}}} \quad (3)$$

where R_{vertical} and $R_{\mathrm{horizontal}}$ are the averaged firing rates during vertical and horizontal stimuli in the correct or incorrect (fig. S8B) trials. This *d*-prime for orientation discriminability, in the strict sense, was recalculated in the trials of the same movements (push or pull) by including not only correct but also incorrect trials (fig. S8A). For comparison, the *d*-prime was also calculated using the average firing rates during the grating presentations in the push and pull trials, R_{push} and R_{pull}, in presenting the same orientation (fig. S8A). For calculating *d*-prime, the averages were calculated in each 0.25-s bin sliding at 0.05-s step for the visual response analysis window. Then, each neuron was assigned the maximum *d*-prime value of all bins (*36*). The *d*-prime value was calculated at each contrast. We analyzed the data containing more than 15 trials (≥15) in each condition. Chance-level distribution was also calculated by randomly swapping vertical and horizontal trials after equalizing the trial number between vertical and horizontal stimuli (the smaller number of trials was adopted) and resampling the activities in the trials 100 times every neuron.

Decoder analysis with population activity (nearest-centroid decoder)

For each session (≥15 trials in this analysis) in each experimental group (task, passive, or anesthetized), 12 neurons were randomly extracted from neuronal populations recorded simultaneously, and decoder analysis was performed on 100 iterations. For this analysis, population activities obtained from WS and NS neurons, consisting of not only enhanced-type but also depressed-type and nonresponsive neurons (see Fig. 1E), were pooled. The population size was determined by considering the decoder accuracy and ensuring the number of sessions (fig. S9, D to F, left).

We adopted the nearest-centroid classifier (*36*, *37*). For calculation of the decoder, activities in correct trials were used. The neuronal population response in each trial was represented as a 24-dimensional vector [12 neurons × 2 time points (0 to 0.5 s and 0.5 to 1.0 s after the onset of grating stimuli, corresponding to the 2-Hz temporal frequency of drifting gratings)]. The centroid for vertical or horizontal stimuli at every contrast was calculated by averaging the population response vectors across all trials, excluding the test trial. To decode the stimulus orientation in the contrast-matched condition, the vector in the test trial was compared with the two centroids calculated at the same contrast as in the test trial. If the vector was closer to the centroid for the same orientation as the presented stimulus, then the decoding was judged as correct. This procedure was performed for all trials every iteration of 12-neuron extraction, and it was also repeated on 100 iterations for each session. Then, the decoder accuracy was assessed by the probability of correct trials. In some analysis, only visually responsive neurons were used (fig. S9A), or the bin width (4× 0.25 s or 1× 1 s) was changed (fig. S9C).

To evaluate the distribution of information regarding orientations across neurons (*36*), we calculated the decoder accuracy after removing neurons one by one, in descending order according to their contribution to the accuracy. The contribution of each neuron was determined by the drop in the decoder accuracy after removing that neuron (fig. S9, D to F, right).

The separation of vertical- and horizontal-orientation representations was evaluated by the mean square Euclidean distance between the two centroids across 100 iterations, divided by the degree number in the vector (24 dimensions) (*36*). The trial-to-trial variability for each stimulus orientation was calculated as the total variance by summing the diagonal of the covariance matrix of the population vector (*36*). The variance was averaged across 100 iterations for each orientation, and then these variances were averaged.

To examine the correlation between decoder accuracy and behavioral choice, the decoder accuracies between the test trials of correct and incorrect choices were compared for each session. The decoder was calculated on the basis of the population activity in correct-choice trials (Fig. 6C). Furthermore, we compared the locations of the population vectors between correct and incorrect test trials on the "discrimination axis" connecting vertical and horizontal centroids. To this end, we calculated the inner products between the population vectors in the test trials and the unit vector from the vertical to the horizontal centroid for projecting the test trial vectors on the axis. Then, these distances in the test trials were normalized by the distance between vertical and horizontal centroids. The distances were calculated for every iteration and averaged across sessions (Fig. 6D).

To examine the contributions of low or high contrast–preferring neurons to the decoder accuracy, the decoder was calculated from neuronal population (12 neurons) without the respective contrast-preferring neurons (Fig. 6, E and F). The decoder accuracies before and after were compared by excluding low or high contrast–preferring neurons in the same sessions that had at least a low or high contrast–preferring neuron and more than 12 neurons (≥12) even without the respective contrast-preferring neurons. When high contrast–preferring neurons were removed, the number of low contrast–preferring neurons in the population increased, and vice versa.

To explore contrast dependence, the orientation was decoded using the decoder calculated from population activities at a different contrast than that of the test trial (the contrast-unmatched condition). We then compared the decoder accuracies between contrast-matched and contrast-unmatched conditions (Fig. 6, G to I).

Multiple linear regression analysis

$$y = \beta_0 + \beta_1 x_1 + \beta_2 x_2 + \cdots + \beta_5 x_5 \quad (4)$$

Multiple linear regression (*75*) in the above calculation was used to estimate the relationship between visual responses (y) of a neuron for the first 1 s during the grating in the trial t and various factors (x_1, x_2, ⋯, x_5). All the factors except for constant term (1) and visual responses were z scored to perform comparisons of coefficient magnitudes (β_0, β_1, β_2, ⋯, β_5). The data per trial were resampled 10,000 times with the bootstrap method in each neuron, and regression coefficients for each resampled data set were calculated. Then, we randomly replaced the relationship between visual responses and various factors for each resampled data point. After gathering the data from all the neurons, we calculated the significance (two-sided P values) of the regression coefficients by doubling the fraction of the shuffled bootstrapped distribution that were larger or smaller (the direction far from the median value of the shuffled data) than the median value of the real bootstrapped data.

Data analysis of LFPs

LFPs were recorded at the same time as multiple single-unit recordings at a sampling rate of 20 kHz and then down-sampled at 1 kHz. LFPs recorded using a channel of the tetrode were analyzed. The recorded traces (band-pass filter, 1 to 5 kHz) were low-pass–filtered (<200 Hz; the final, 1 to 200 Hz) with a digital filter constructed via the Parks-McClellan equiripple finite impulse response (FIR) filter design with the MATLAB function designfilt. Because the constant time delay is generated using this digital filter, the LFP traces were shifted to counteract this time delay.

Spectral analysis

We normalized the filtered LFP signals with the z score and then whitened the LFP (*29*, *50*). We adopted a low-order (order = 3) autoregressive (AR) model to equalize the variance across frequency bins and decrease frequency leakage during the spectral analysis. Because this model essentially fits the "pink" shape (~1/f) of the spectrum, the pink component can be subtracted. The Levinson-Durbin recursion method was used to fit the AR model, and then the coefficients (A_k) of the model for the original time series data (X_t) were estimated (*50*). The residuals, which were used during the spectral analysis, were calculated as follows

$$\Delta X_t = X_t - \sum_{k=1}^{3} X_{t-k} A_k \quad (5)$$

The power spectrum was calculated using the multitaper estimation method [TW (the time-bandwidth product) = 3, K (the number of tapers) = 5] for 9-s data segments (3 s before to 6 s following visual grating onset), after removing the 60-Hz line noise using the Chronux toolbox for MATLAB (http://chronux.org) (*76*). Here, the data during the vertical and horizontal stimuli were mixed. In the time-frequency spectral analysis, we calculated the continuous power spectrograms of the segmented LFPs using a 0.5-s sliding window at a 0.02-s step. The power at each frequency and time point was normalized using the mean power across all frequency bands (1 to 90 Hz) and the baseline period (0.5 to 1.5 s before cue stimulus onset), unless otherwise specifically noted. This power was averaged across recorded channels and sessions as well as across rats and represented in the pseudo-color plot.

Spike-LFP PPC

From the filtered (1 to 200 Hz) LFP traces, the 60-Hz line noise was removed as stated above. The paired data between the spike train of an analyzed neuron [ongoing activities (all averaged) > 1 Hz] and the LFP traces, which were recorded at the tetrode (a channel per a tetrode) other than that recording the spikes, during the gratings of the preferred orientation for the neuron, were used to calculate the PPC (*42*, *50*). The PPC was defined as

$$\mathrm{PPC} = \frac{2}{N(N-1)} \sum_{j=1}^{N-1} \sum_{k=(j+1)}^{N} f(\theta_j, \theta_k) \quad (6)$$

$$f(\theta_j, \theta_k) = \cos(\theta_j - \theta_k) = \cos(\theta_j)\cos(\theta_k) + \sin(\theta_j)\sin(\theta_k) \quad (7)$$

where θ_j and θ_k are corresponding LFP phases of the jth and kth spikes in a neuron. N is the total number of spikes. The PPC spectra for each unit were calculated by using the FieldTrip toolbox for MATLAB (www.fieldtriptoolbox.org/) (*42*).

A time window of 4 s during gratings was used to calculate the visually induced PPC, while 0 to 1.5 s before the cue onset was used to calculate the baseline PPC. Visually induced change of PPC was defined as

$$\Delta\mathrm{PPC} = \mathrm{PPC}_{\mathrm{grating}} - \mathrm{PPC}_{\mathrm{baseline}} \quad (8)$$

LFP phase preference of spikes

The filtered (1 to 200 Hz) LFP was refiltered using an infinite impulse response Butterworth filter at 18 to 30 Hz (beta band). Because the time delay is generated using this filter, the traces were bidirectionally filtered (2× 10th order) with the MATLAB function filtfilt. Instantaneous beta phases were estimated using the Hilbert transformation of the filtered signals. Uniformity of the phase of spikes was evaluated by the Rayleigh test (*77*) using the CircStat toolbox for MATLAB (www.jstatsoft.org/v31/i10) (*78*). We calculated the statistics $Z = R^2/n$ (R, resultant length; n, sample size) and variance-stabilized log(Z) for significance test. For significantly modulated ($P < 0.01$) neurons, the peak of phase histogram was assigned as the preferred phase in each neuron.

Visually evoked LFPs (VEPs)

The filtered (1 to 200 Hz) LFPs were aligned to the grating onset and averaged without distinguishing between vertical and horizontal stimuli. Here, the LFPs were recorded from layer 5, not layer 4, because LFPs and spikes were simultaneously recorded using the same probe. The magnitude was evaluated as the trough-to-peak difference. We searched the trough for 1 to 150 ms after grating onset and the peak over the duration between the trough and 250 ms after grating onset. These magnitudes were averaged across the tetrodes and sessions and were finally averaged across rats.

Statistical analysis

Data are expressed as means ± SEM. MATLAB (mostly, R2018a; MathWorks) and SigmaPlot (version 14.0; Systat Software) were used for quantifications and statistical analyses. Regarding data distributions, no assumptions of normality were imposed, and nonparametric statistical tests were used. Two-sample Kolmogorov-Smirnov test was performed to evaluate differences between two distributions of certain features in firing rates. In comparisons between real and shuffled data, we performed one-sample Kolmogorov-Smirnov test to compare to hypothesized shuffled distributions because of the huge number of shuffled data bootstrapped 10,000 times. The Kuiper's

test was used to evaluate differences between two distributions for circular phase data using the MATLAB Toolbox for Circular Statistics (*78*). The Wilcoxon rank sum test or signed-rank test was performed to compare differences of unpaired or paired data, respectively. One-sample Wilcoxon signed-rank test was performed to check whether tested data originated from a distribution with a median value. If we confirmed the significant differences in multiple statistical tests, we then tested whether the significance was generated by chance, using Holm correction. In Holm correction, the P values of respective statistical tests were sorted as $P_1 \leq P_2 \leq \ldots P_i \leq \ldots P_M$, where M is the number of statistical tests. Tests from 1 to the maximum order i, such that $P_i < \alpha/(M + 1 - i)$, were accepted at a significance level α. We used two significance levels, $\alpha = 0.01$ and 0.05. Comparisons among three or more unpaired or paired groups were performed by Kruskal-Wallis test or Friedman's test, respectively. If the significance of Kruskal-Wallis test remained after the correction, then we performed Dunn's test among all pairs. For comparison of ratios, chi-square test was performed.

Statistical tests were two sided, and $P < 0.05$ was considered statistically significant, except in the case of Rayleigh test for phase modulation. No statistical methods were used to predetermine sample sizes, but our sample sizes are similar to those generally used in the field (*35*). No randomization or blinding was performed during experiments or data analysis. Box plots indicate the median (black or colored line) of the index values, the 25th and 75th percentiles (box), and the 10th and 90th percentiles (error bars, except for multiple linear regression analysis). Exact P values are expressed only for $P \geq 0.001$, except in the case of the bootstrap test for proportions of contrast-preferring neurons (minimum P value of 0.0001).

SUPPLEMENTARY MATERIALS

Supplementary material for this article is available at https://science.org/doi/10.1126/sciadv.abj9976

View/request a protocol for this paper from *Bio-protocol*.

REFERENCES AND NOTES

1. A. Karni, D. Sagi, Where practice makes perfect in texture discrimination: Evidence for primary visual cortex plasticity. *Proc. Natl. Acad. Sci. U.S.A.* **88**, 4966–4970 (1991).
2. W. Li, V. Piech, C. D. Gilbert, Learning to link visual contours. *Neuron* **57**, 442–451 (2008).
3. N. K. Logothetis, J. Pauls, T. Poggio, Shape representation in the inferior temporal cortex of monkeys. *Curr. Biol.* **5**, 552–563 (1995).
4. P. T. Sowden, D. Rose, I. R. Davies, Perceptual learning of luminance contrast detection: Specific for spatial frequency and retinal location but not orientation. *Vis. Res.* **42**, 1249–1258 (2002).
5. C. S. Furmanski, D. Schluppeck, S. A. Engel, Learning strengthens the response of primary visual cortex to simple patterns. *Curr. Biol.* **14**, 573–578 (2004).
6. Y. Yotsumoto, T. Watanabe, Y. Sasaki, Different dynamics of performance and brain activation in the time course of perceptual learning. *Neuron* **57**, 827–833 (2008).
7. M. Y. Frenkel, N. B. Sawtell, A. C. Diogo, B. Yoon, R. L. Neve, M. F. Bear, Instructive effect of visual experience in mouse visual cortex. *Neuron* **51**, 339–349 (2006).
8. A. G. Khan, J. Poort, A. Chadwick, A. Blot, M. Sahani, T. D. Mrsic-Flogel, S. B. Hofer, Distinct learning-induced changes in stimulus selectivity and interactions of GABAergic interneuron classes in visual cortex. *Nat. Neurosci.* **21**, 851–859 (2018).
9. H. Makino, T. Komiyama, Learning enhances the relative impact of top-down processing in the visual cortex. *Nat. Neurosci.* **18**, 1116–1122 (2015).
10. J. M. Pakan, V. Francioni, N. L. Rochefort, Action and learning shape the activity of neuronal circuits in the visual cortex. *Curr. Opin. Neurobiol.* **52**, 88–97 (2018).
11. J. Poort, A. G. Khan, M. Pachitariu, A. Nemri, I. Orsolic, J. Krupic, M. Bauza, M. Sahani, G. B. Keller, T. D. Mrsic-Flogel, S. B. Hofer, Learning enhances sensory and multiple non-sensory representations in primary visual cortex. *Neuron* **86**, 1478–1490 (2015).
12. T. Hua, P. Bao, C. B. Huang, Z. Wang, J. Xu, Y. Zhou, Z. L. Lu, Perceptual learning improves contrast sensitivity of V1 neurons in cats. *Curr. Biol.* **20**, 887–894 (2010).
13. H. Adesnik, Synaptic mechanisms of feature coding in the visual cortex of awake mice. *Neuron* **95**, 1147–1159.e4 (2017).
14. L. Busse, A. Ayaz, N. T. Dhruv, S. Katzner, A. B. Saleem, M. L. Scholvinck, A. D. Zaharia, M. Carandini, The detection of visual contrast in the behaving mouse. *J. Neurosci.* **31**, 11351–11361 (2011).
15. C. M. Niell, M. P. Stryker, Highly selective receptive fields in mouse visual cortex. *J. Neurosci.* **28**, 7520–7536 (2008).
16. G. Sclar, R. D. Freeman, Orientation selectivity in the cat's striate cortex is invariant with stimulus contrast. *Exp. Brain Res.* **46**, 457–461 (1982).
17. J. W. Peirce, The potential importance of saturating and supersaturating contrast response functions in visual cortex. *J. Vis.* **7**, 13 (2007).
18. I. Sani, E. Santandrea, A. Golzar, M. C. Morrone, L. Chelazzi, Selective tuning for contrast in macaque area V4. *J. Neurosci.* **33**, 18583–18596 (2013).
19. K. Cohen-Kashi Malina, E. Tsivourakis, D. Kushinsky, D. Apelblat, S. Shtiglitz, E. Zohar, M. Sokoletsky, G. I. Tasaka, A. Mizrahi, I. Lampl, I. Spiegel, NDNF interneurons in layer 1 gain-modulate whole cortical columns according to an animal's behavioral state. *Neuron* **109**, 2150–2164.e5 (2021).
20. S. Durand, R. Iyer, K. Mizuseki, S. de Vries, S. Mihalas, R. C. Reid, A comparison of visual response properties in the lateral geniculate nucleus and primary visual cortex of awake and anesthetized mice. *J. Neurosci.* **36**, 12144–12156 (2016).
21. S. Lee, J. Park, S. M. Smirnakis, Internal gain modulations, but not changes in stimulus contrast, preserve the neural code. *J. Neurosci.* **39**, 1671–1687 (2019).
22. D. J. Millman, G. K. Ocker, S. Caldejon, I. Kato, J. D. Larkin, E. K. Lee, J. Luviano, C. Nayan, T. V. Nguyen, K. North, S. Seid, C. White, J. Lecoq, C. Reid, M. A. Buice, S. E. de Vries, VIP interneurons in mouse primary visual cortex selectively enhance responses to weak but specific stimuli. *eLife* **9**, e55130 (2020).
23. S. Zhang, M. Xu, T. Kamigaki, J. P. Hoang Do, W. C. Chang, S. Jenvay, K. Miyamichi, L. Luo, Y. Dan, Selective attention. Long-range and local circuits for top-down modulation of visual cortex processing. *Science* **345**, 660–665 (2014).
24. L. Pinto, M. J. Goard, D. Estandian, M. Xu, A. C. Kwan, S. H. Lee, T. C. Harrison, G. Feng, Y. Dan, Fast modulation of visual perception by basal forebrain cholinergic neurons. *Nat. Neurosci.* **16**, 1857–1863 (2013).
25. S. H. Lee, A. C. Kwan, S. Zhang, V. Phoumthipphavong, J. G. Flannery, S. C. Masmanidis, H. Taniguchi, Z. J. Huang, F. Zhang, E. S. Boyden, K. Deisseroth, Y. Dan, Activation of specific interneurons improves V1 feature selectivity and visual perception. *Nature* **488**, 379–383 (2012).
26. J. J. Cone, M. D. Scantlen, M. H. Histed, J. H. R. Maunsell, Different inhibitory interneuron cell classes make distinct contributions to visual contrast perception. *eNeuro* **6**, ENEURO.0337–ENEU18.2019 (2019).
27. M. J. Goard, G. N. Pho, J. Woodson, M. Sur, Distinct roles of visual, parietal, and frontal motor cortices in memory-guided sensorimotor decisions. *eLife* **5**, e13764 (2016).
28. A. J. Keller, R. Houlton, B. M. Kampa, N. A. Lesica, T. D. Mrsic-Flogel, G. B. Keller, F. Helmchen, Stimulus relevance modulates contrast adaptation in visual cortex. *eLife* **6**, e21589 (2017).
29. C. M. Niell, M. P. Stryker, Modulation of visual responses by behavioral state in mouse visual cortex. *Neuron* **65**, 472–479 (2010).
30. D. M. Piscopo, R. N. El-Danaf, A. D. Huberman, C. M. Niell, Diverse visual features encoded in mouse lateral geniculate nucleus. *J. Neurosci.* **33**, 4642–4656 (2013).
31. M. Vinck, R. Batista-Brito, U. Knoblich, J. A. Cardin, Arousal and locomotion make distinct contributions to cortical activity patterns and visual encoding. *Neuron* **86**, 740–754 (2015).
32. S. A. Baccus, M. Meister, Fast and slow contrast adaptation in retinal circuitry. *Neuron* **36**, 909–919 (2002).
33. R. H. Masland, The fundamental plan of the retina. *Nat. Neurosci.* **4**, 877–886 (2001).
34. A. Mason, A. Larkman, Correlations between morphology and electrophysiology of pyramidal neurons in slices of rat visual cortex. II. Electrophysiology. *J. Neurosci.* **10**, 1415–1428 (1990).
35. A. Saiki, Y. Sakai, R. Fukabori, S. Soma, J. Yoshida, M. Kawabata, H. Yawo, K. Kobayashi, M. Kimura, Y. Isomura, In vivo spiking dynamics of intra- and extratelencephalic projection neurons in rat motor cortex. *Cereb. Cortex* **28**, 1024–1038 (2018).
36. M. W. Chu, W. L. Li, T. Komiyama, Balancing the robustness and efficiency of odor representations during learning. *Neuron* **92**, 174–186 (2016).
37. H. K. Kato, M. W. Chu, J. S. Isaacson, T. Komiyama, Dynamic sensory representations in the olfactory bulb: Modulation by wakefulness and experience. *Neuron* **76**, 962–975 (2012).
38. J. H. Marshel, Y. S. Kim, T. A. Machado, S. Quirin, B. Benson, J. Kadmon, C. Raja, A. Chibukhchyan, C. Ramakrishnan, M. Inoue, J. C. Shane, D. J. McKnight, S. Yoshizawa, H. E. Kato, S. Ganguli, K. Deisseroth, Cortical layer-specific critical dynamics triggering perception. *Science* **365**, eaaw5202 (2019).
39. T. Yoshida, K. Ohki, Natural images are reliably represented by sparse and variable populations of neurons in visual cortex. *Nat. Commun.* **11**, 872 (2020).
40. B. Haider, A. Duque, A. R. Hasenstaub, Y. Yu, D. A. McCormick, Enhancement of visual responsiveness by spontaneous local network activity in vivo. *J. Neurophysiol.* **97**, 4186–4202 (2007).

41. S. Mahon, S. Charpier, Bidirectional plasticity of intrinsic excitability controls sensory inputs efficiency in layer 5 barrel cortex neurons in vivo. *J. Neurosci.* **32**, 11377–11389 (2012).
42. M. Vinck, M. van Wingerden, T. Womelsdorf, P. Fries, C. M. Pennartz, The pairwise phase consistency: A bias-free measure of rhythmic neuronal synchronization. *NeuroImage* **51**, 112–122 (2010).
43. A. K. Engel, P. Fries, W. Singer, Dynamic predictions: Oscillations and synchrony in top-down processing. *Nat. Rev. Neurosci.* **2**, 704–716 (2001).
44. J. A. Cardin, M. Carlen, K. Meletis, U. Knoblich, F. Zhang, K. Deisseroth, L. H. Tsai, C. I. Moore, Driving fast-spiking cells induces gamma rhythm and controls sensory responses. *Nature* **459**, 663–667 (2009).
45. L. Carrillo-Reid, W. Yang, Y. Bando, D. S. Peterka, R. Yuste, Imprinting and recalling cortical ensembles. *Science* **353**, 691–694 (2016).
46. P. Fries, D. Nikolic, W. Singer, The gamma cycle. *Trends Neurosci.* **30**, 309–316 (2007).
47. V. S. Sohal, How close are we to understanding what (if anything) γ oscillations do in cortical circuits? *J. Neurosci.* **36**, 10489–10495 (2016).
48. D. B. Rubin, S. D. Van Hooser, K. D. Miller, The stabilized supralinear network: A unifying circuit motif underlying multi-input integration in sensory cortex. *Neuron* **85**, 402–417 (2015).
49. S. Sadeh, C. Clopath, Inhibitory stabilization and cortical computation. *Nat. Rev. Neurosci.* **22**, 21–37 (2021).
50. G. Chen, Y. Zhang, X. Li, X. Zhao, Q. Ye, Y. Lin, H. W. Tao, M. J. Rasch, X. Zhang, Distinct inhibitory circuits orchestrate cortical beta and gamma band oscillations. *Neuron* **96**, 1403–1418.e6 (2017).
51. H. Adesnik, W. Bruns, H. Taniguchi, Z. J. Huang, M. Scanziani, A neural circuit for spatial summation in visual cortex. *Nature* **490**, 226–231 (2012).
52. G. C. DeAngelis, R. D. Freeman, I. Ohzawa, Length and width tuning of neurons in the cat's primary visual cortex. *J. Neurophysiol.* **71**, 347–374 (1994).
53. A. Vaiceliunaite, S. Erisken, F. Franzen, S. Katzner, L. Busse, Spatial integration in mouse primary visual cortex. *J. Neurophysiol.* **110**, 964–972 (2013).
54. M. T. Alkire, A. G. Hudetz, G. Tononi, Consciousness and anesthesia. *Science* **322**, 876–880 (2008).
55. A. J. Keller, M. M. Roth, M. Scanziani, Feedback generates a second receptive field in neurons of the visual cortex. *Nature* **582**, 545–549 (2020).
56. M. Sarter, B. Givens, J. P. Bruno, The cognitive neuroscience of sustained attention: Where top-down meets bottom-up. *Brain Res. Rev.* **35**, 146–160 (2001).
57. A. K. Engel, P. Fries, Beta-band oscillations—Signalling the status quo? *Curr. Opin. Neurobiol.* **20**, 156–165 (2010).
58. A. G. Khan, S. B. Hofer, Contextual signals in visual cortex. *Curr. Opin. Neurobiol.* **52**, 131–138 (2018).
59. H. Sato, Y. Hata, H. Masui, T. Tsumoto, A functional role of cholinergic innervation to neurons in the cat visual cortex. *J. Neurophysiol.* **58**, 765–780 (1987).
60. S. Manita, T. Suzuki, C. Homma, T. Matsumoto, M. Odagawa, K. Yamada, K. Ota, C. Matsubara, A. Inutsuka, M. Sato, M. Ohkura, A. Yamanaka, Y. Yanagawa, J. Nakai, Y. Hayashi, M. E. Larkum, M. Murayama, A top-down cortical circuit for accurate sensory perception. *Neuron* **86**, 1304–1316 (2015).
61. M. Goard, Y. Dan, Basal forebrain activation enhances cortical coding of natural scenes. *Nat. Neurosci.* **12**, 1444–1449 (2009).
62. W. P. Dai, D. Zhou, D. W. McLaughlin, D. Cai, Mechanisms underlying contrast-dependent orientation selectivity in mouse V1. *Proc. Natl. Acad. Sci. U.S.A.* **115**, 11619–11624 (2018).
63. Y. T. Li, W. P. Ma, L. Y. Li, L. A. Ibrahim, S. Z. Wang, H. W. Tao, Broadening of inhibitory tuning underlies contrast-dependent sharpening of orientation selectivity in mouse visual cortex. *J. Neurosci.* **32**, 16466–16477 (2012).
64. C. E. Shannon, A mathematical theory of communication. *Bell Syst. Tech. J.* **27**, 379–423 (1948).
65. R. Kimura, A. Saiki, Y. Fujiwara-Tsukamoto, F. Ohkubo, K. Kitamura, M. Matsuzaki, Y. Sakai, Y. Isomura, Reinforcing operandum: Rapid and reliable learning of skilled forelimb movements by head-fixed rodents. *J. Neurophysiol.* **108**, 1781–1792 (2012).
66. R. Kimura, A. Saiki, Y. Fujiwara-Tsukamoto, Y. Sakai, Y. Isomura, Large-scale analysis reveals populational contributions of cortical spike rate and synchrony to behavioural functions. *J. Physiol.* **595**, 385–413 (2017).
67. M. Long, W. Jiang, D. Liu, H. Yao, Contrast-dependent orientation discrimination in the mouse. *Sci. Rep.* **5**, 15830 (2015).
68. D. H. Brainard, The psychophysics toolbox. *Spat. Vis.* **10**, 433–436 (1997).
69. N. Suematsu, T. Naito, H. Sato, Relationship between orientation sensitivity and spatiotemporal receptive field structures of neurons in the cat lateral geniculate nucleus. *Neural Netw.* **35**, 10–20 (2012).
70. T. Takekawa, Y. Isomura, T. Fukai, Accurate spike sorting for multi-unit recordings. *Eur. J. Neurosci.* **31**, 263–272 (2010).
71. T. Takekawa, Y. Isomura, T. Fukai, Spike sorting of heterogeneous neuron types by multimodality-weighted PCA and explicit robust variational Bayes. *Front. Neuroinform.* **6**, 5 (2012).
72. L. Hazan, M. Zugaro, G. Buzsaki, Klusters, NeuroScope, NDManager: A free software suite for neurophysiological data processing and visualization. *J. Neurosci. Methods* **155**, 207–216 (2006).
73. M. G. Shuler, M. F. Bear, Reward timing in the primary visual cortex. *Science* **311**, 1606–1609 (2006).
74. P. Bartho, H. Hirase, L. Monconduit, M. Zugaro, K. D. Harris, G. Buzsaki, Characterization of neocortical principal cells and interneurons by network interactions and extracellular features. *J. Neurophysiol.* **92**, 600–608 (2004).
75. S. N. Chettih, C. D. Harvey, Single-neuron perturbations reveal feature-specific competition in V1. *Nature* **567**, 334–340 (2019).
76. H. Bokil, K. Purpura, J. M. Schoffelen, D. Thomson, P. Mitra, Comparing spectra and coherences for groups of unequal size. *J. Neurosci. Methods* **159**, 337–345 (2007).
77. A. Sirota, S. Montgomery, S. Fujisawa, Y. Isomura, M. Zugaro, G. Buzsaki, Entrainment of neocortical neurons and gamma oscillations by the hippocampal theta rhythm. *Neuron* **60**, 683–697 (2008).
78. P. Berens, CircStat: A MATLAB Toolbox for circular statistics. *J. Stat. Softw.* **31**, 1–21 (2009).
79. G. Paxinos, C. Watson, *The Rat Brain in Stereotaxic Coordinates* (Academic Press, ed. 6, 2007).
80. N. I. Fisher, *Statistical Analysis of Circular Data* (Cambridge Univ. Press, 1995).

Acknowledgments: We thank K. Ohki (The University of Tokyo) for the encouragement. We thank Y. Komatsu (NIPS), Y. Isomura (Tokyo Medical and Dental University), and Y. Sakai (Tamagawa University) for helpful advice. We thank previous and current members of the Yoshimura laboratory (NIPS) for important discussions. We thank T. Naito (Osaka University) and N. Suematsu (Kyoto Sangyo University) for providing us with the original version of a computer program for visual stimulation. We thank A. Nambu (NIPS) and S. Oda (NIPS) in regard to the histological experiments. **Funding:** This work was supported by KAKENHI (26115521, 26830019, 17KT0115, 18H05143, 18K06537, 20H05077, and 21K06447), the JST FOREST Program (JPMJFR2041), the Hori Sciences and Arts Foundation, and the Public Foundation of Chubu Science and Technology Center to R.K. and KAKENHI (16H01625, 16H06460, 18H02547, and 21H02600) to Y.Y. **Author contributions:** R.K. and Y.Y. designed the research. R.K. performed the experiments. R.K. analyzed the data. R.K. and Y.Y. interpreted the data. R.K. and Y.Y. wrote and revised the manuscript. **Competing interests:** The authors declare that they have no competing interests. **Data and materials availability:** All data needed to evaluate the conclusions in the paper are present in the paper and/or the Supplementary Materials.

Submitted 15 June 2021
Accepted 7 October 2021
Published 26 November 2021
10.1126/sciadv.abj9976